HHS Public Access

Author manuscript

Neurobiol Dis. Author manuscript; available in PMC 2021 January 01.

Published in final edited form as:

Neurobiol Dis. 2021 January ; 147: 105153. doi:10.1016/j.nbd.2020.105153.

LAR inhibitory peptide promotes recovery of diaphragm function and multiple forms of respiratory neural circuit plasticity after cervical spinal cord injury

Lan Cheng[a], **Armin Sami**[a], **Biswarup Ghosh**[a], **Mark W. Urban**[a], **Nicolette M. Heinsinger**[a], **Sophia S. Liang**[a], **George M. Smith**[b], **Megan C. Wright**[c], **Shuxin Li**[d], **Angelo C. Lepore**[a,*]

[a]Department of Neuroscience, Vickie and Jack Farber Institute for Neuroscience·, Sidney Kimmel Medical College at Thomas Jefferson University, Philadelphia, PA 19107, United States of America

[b]Department of Neuroscience, Shriners Hospitals for Pediatric Research Center, Temple University School of Medicine, 3500 North Broad Street, Philadelphia, PA 19140-5104, United States of America

[c]Department of Biology, Arcadia University, Glenside, PA 19038, United States of America

[d]Department of Anatomy and Cell Biology, Shriners Hospitals for Pediatric Research Center, Temple University School of Medicine, 3500 North Broad Street, Philadelphia, PA 19140-5104, United States of America

Abstract

Chondroitin sulfate proteoglycans (CSPGs), up-regulated in and around the lesion after traumatic spinal cord injury (SCI), are key extracellular matrix inhibitory molecules that limit axon growth and consequent recovery of function. CSPG-mediated inhibition occurs via interactions with axonal receptors, including leukocyte common antigen- related (LAR) phosphatase. We tested the effects of a novel LAR inhibitory peptide in rats after hemisection at cervical level 2, a SCI model in which bulbospinal inspiratory neural circuitry originating in the medullary rostral ventral respiratory group (rVRG) becomes disconnected from phrenic motor neuron (PhMN) targets in cervical spinal cord, resulting in persistent partial-to-complete diaphragm paralysis. LAR peptide was delivered by a soaked gelfoam, which was placed directly over the injury site immediately after C2 hemisection and replaced at 1 week post-injury. Axotomized rVRG axons originating in ipsilateral medulla or spared rVRG fibers originating in contralateral medulla were separately assessed by anterograde tracing via AAV2-mCherry injection into rVRG. At 8 weeks post-hemisection, LAR peptide significantly improved ipsilateral hemidiaphragm function, as assessed in vivo with electromyography recordings. LAR peptide promoted robust regeneration of ipsilateral-originating rVRG axons into and through the lesion site and into intact caudal spinal

*Corresponding author at: Department of Neuroscience, Vickie and Jack Farber Institute for Neuroscience, Sidney Kimmel Medical College at Thomas Jefferson University, 233 South 10th Street, BLSB 245, Philadelphia, PA 19107, United States of America. angelo.lepore@jefferson.edu (A.C. Lepore).

Declaration of Competing Interest

None - The authors declare no financial or other competing interests.

cord to reach PhMNs located at C3-C5 levels. Furthermore, regenerating rVRG axons re-established putative monosynaptic connections with their PhMNs targets. In addition, LAR peptide stimulated robust sprouting of both modulatory serotonergic axons and contralateral-originating rVRG fibers within the PhMN pool ipsilateral/ caudal to the hemisection. Our study demonstrates that targeting LAR-based axon growth inhibition promotes multiple forms of respiratory neural circuit plasticity and provides a new peptide-based therapeutic strategy to ameliorate the devastating respiratory consequences of SCI.

Keywords

CSPG; ECM; LAR; SCI; Breathing; Functional recovery

1. Introduction

Following traumatic spinal cord injury (SCI), functional deficits vary depending on the anatomical location, type and severity of the insult, as well as on the specific neural circuits affected (Ahuja et al., 2017). Approximately half of all SCI cases are located within the cervical spinal cord, with many of these individuals suffering from debilitating and persistent respiratory deficits and relying on mechanical ventilation for the remainder of their lives (Lane et al., 2008a). Despite surgical intervention (e.g. vertebral bone stabilization), supportive and rehabilitation interventions, individuals affected by SCI carry a life-long risk for complications arising from motor, sensory and autonomic deficits. The limited ability of the injured spinal cord to repair itself remains a major barrier to achieving meaningful recovery of function after SCI. In particular, the severed axonal projections of damaged neurons are not capable of mounting a robust regenerative response after SCI, resulting in permanent disconnection of the neural circuits responsible for mediating various behaviors.

Understanding the mechanisms that can drive a successful axon regrowth process after central nervous system (CNS) injury is critical to develop methods to therapeutically promote recovery of function in SCI and other neurological diseases. Without any intervention, spontaneous axon growth is extremely limited after SCI due in part to neuronalextrinsic factors present in the injured CNS, including reactive scarring (Burda and Sofroniew, 2014), acellular cystic cavity formation (Kamada et al., 2011), excessive and persistent neuroinflammation (Zhu et al., 2015), expression of various axon-growth inhibitory molecules (Beller and Snow, 2014), absence of trophic support (Robinson and Lu, 2017), and the inadequate spatiotemporal production of axon guidance molecules to appropriately sculpt newly formed circuits (Sperry, 1963). In addition to environmental factors, axon growth in the injured adult CNS is limited by a number of important neuronal-intrinsic mechanisms such as the PTEN-mTOR signaling axis (Park et al., 2010).

The extracellular matrix (ECM) plays essential roles in a variety of biological processes within both the intact and diseased nervous system such as cell migration, proliferation and differentiation. The ECM is also is a major source of axon growth inhibitors (Barros et al., 2011; Franco and Muller, 2011). In the CNS, the ECM is comprised of a number of different

molecules, including chondroitin sulfate proteoglycans (CSPGs), non-collagenous glycoproteins, fibrillar collagens and hyaluronan (Benarroch, 2015; Fawcett, 2015). CSPGs are normally expressed in the intact spinal cord where they contribute to fundamental cellular processes. CSPGs can be significantly upregulated after CNS injury, resulting in growth inhibition of both damaged and spared axon populations (Lang et al., 2015; Tran et al., 2018). Following insults to the CNS, increased CSPG secretion occurs in a number of cell types such as astrocytes, fibroblasts, pericytes and inflammatory cells, in particular within reactive scar tissue (Sharma et al., 2012). This upregulated CSPG expression mediates axon growth inhibition by signaling through receptors located on the membrane of axons, thereby limiting CNS plasticity and repair (Bartus et al., 2012; Kwok et al., 2011; Xu et al., 2015). CSPGs can also induce caspase 3-mediated cell death in mature oligodendrocytes and in populations of neural precursors such as oligodendrocyte progenitor cells (Dyck et al., 2019). By selectively cleaving the glycosaminoglycan (GAG) side chains of CSPGs (which are responsible for mediating a major portion of the axonal effects of CSPGs) via introduction of the bacterial enzyme chondroitinase ABC (ChABC), pioneering work has demonstrated that modulating the axon growth inhibitory impact of CSPGs after SCI can promote growth of injured and spared axons and some degree of functional recovery (Alilain et al., 2011; Bradbury et al., 2002; Garcia-Alias et al., 2009; James et al., 2015; Ramer et al., 2014). CSPGs may therefore be an important therapeutic target for promoting repair following SCI.

Structurally, proteoglycans contain a protein core and GAG side chains (chondroitin sulfate in the case of CSPGs). While it was initially believed that CSPGs mediated their axon growth inhibitory effects by steric hindrance of adhesion molecules that are growth promoting, the transmembrane protein tyrosine phosphatase-sigma (PTPσ) (Fry et al., 2010; Shen et al., 2009) and related phosphatase leukocyte common antigen-related (LAR) (Fisher et al., 2011; Wong et al., 1993; Yang et al., 1999) have been identified as the axonal receptors for the inhibitory actions of CSPGs. In addition to PTPa and LAR, CSPGs can exert axon growth inhibitory effects via signaling through Nogo receptors 1 and 3 (Dickendesher et al., 2012). LAR and PTPσ belong to the type IIa/LAR subfamily of receptor protein tyrosine phosphatases (RPTP), which includes the three vertebrate members LAR, PTPδ and PTPσ (Tonks, 2006). Structurally, LAR RPTP contains an Ig-like domain that binds CSPGs, an extracellular fifth fibronectin type III domain, and an intracellular wedge-shaped helix-loop-helix (Xie et al., 2020). The large extracellular regions of LAR RPTP can interact with additional extracellular ligands besides proteoglycans (e.g. liprin-α, netrin-G ligand-3, TrkB) (Han et al., 2016; Takahashi and Craig, 2013), thereby mediating proteoglycan-regulated processes such as axon guidance and excitatory presynaptic and postsynaptic assembly (Fisher et al., 2011; Shen et al., 2009). CSPGs bind to LAR RPTPs on the axon membrane to regulate a number of intracellular transduction pathways. This signaling can include stimulation of the RhoA kinase pathway and inactivation Akt and Erk pathways (Fisher et al., 2011) to restrict neurite outgrowth (Fisher et al., 2011; Lang et al., 2015; Xu et al., 2015). Deletion of LAR in knockout mice significantly overcomes CSPG-mediated neurite growth inhibition in neuronal culture (Fisher et al., 2011). Similarly, systemic treatment with LAR-targeting inhibitory peptides that block LAR activity in mice with thoracic transection SCI induces significant growth of descending serotonergic axons

and also promotes locomotor functional recovery (Fisher et al., 2011). Additionally, inhibition of LAR promotes oligodendrogenesis from endogenous progenitor cells, attenuates caspase 3-mediated cell death of mature oligodendrocytes, and preserves myelin after SCI (Dyck et al., 2018). Based on this body of work, LAR RPTP is a promising target for interventions that block the effects of CSPGs and provides an opportunity to enhance axon growth after CNS injury.

Respiratory dysfunction is an extremely debilitating outcome of SCI that results in part from disruption of bulbospinal circuitry that controls the diaphragm, a primary muscle of inspiration (Warren et al., 2014). Phrenic motor neurons (PhMNs) located at cervical spinal cord level 3 (C3)-5 (C5) innervate the ipsilateral diaphragm (Lane et al., 2009). These PhMNs receive primarily monosynaptic excitatory drive from rostral ventral respiratory group (rVRG) neurons located in medulla (Zimmer et al., 2007). PhMNs are also connected with rVRG neurons through poly-synaptic circuits involving pre-phrenic interneurons of cervical spinal cord (Lane et al., 2008b; Zholudeva et al., 2017). Cervical SCI damages this descending bulbospinal axon input to the PhMNs. As little growth of damaged axons occurs after SCI, PhMNs remain denervated from their rVRG input, resulting in persistent partial-to-complete diaphragm paralysis.

In a rat model of C2 hemisection-type SCI (Urban et al., 2019a; Urban et al., 2019b; Urban et al., 2018), we explored mechanisms of rVRG-PhMN-diaphragm circuit plasticity that can drive recovery of diaphragm function in response to manipulating axon growth inhibition. Specifically, we administered a novel LAR-targeting sequence-selective inhibitory peptide (abbreviated as LAR peptide) to the injured cervical spinal cord and assessed effects on diaphragm function using in vivo electrophysiological assays. In addition, we examined neuroanatomical effects of LAR inhibition on respiratory neural circuitry using anterograde and retrograde tracing approaches to quantitatively assess regeneration of injured rVRG axons, sprouting of spared rVRG fibers, and monosynaptic connectivity of these rVRG axon populations with PhMN targets located caudal to the lesion site. Furthermore, we took advantage of the observed animal-to-animal variability in LAR peptide-induced functional effects and axon growth responses to perform correlation analyses to explore mechanisms of rVRG-PhMN-diaphragm circuit plasticity responsible for driving recovery of diaphragm function.

2. Results

2.1. C2 hemisection SCI model and experimental design

Hemisection of the cervical level 2 (C2) spinal cord from the midline to lateral edge has been used extensively to study respiratory plasticity following SCI (Bezdudnaya et al., 2017; Mantilla et al., 2017; Streeter et al., 2020). C2 hemisection axotomizes descending bulbospinal pathways originating in the rVRG of the medulla, thereby interrupting their connections to the PhMNs located at cervical levels C3-C5. Thus, a hemiparalysis of the diaphragm occurs ipsilateral to the injury, while the rVRG-PhMN-diaphragm circuit remains intact on the contralateral side. The hemisected animal is able to maintain ventilation due to preservation of both contralateral hemidiaphragm function and other non diaphragm respiratory muscle pathways. C2 hemisection SCI is a powerful experimental model to

mechanistically study plasticity of respiratory neural circuitry using neuroanatomical labeling of various components of this critically important circuit. In addition, various in vivo assays can be employed to assess recovery of diaphragm function in response to experimental manipulations, including therapeutic strategies.

As shown in the experimental timeline (Fig. 1A), a biocompatible gelfoam was soaked with either DMSO vehicle- only control or LAR peptide and was placed directly over the SCI site immediately after C2 hemisection. The gelfoam was then replaced with fresh peptide (or DMSO only) at 1 week post-injury. Two weeks post-SCI, we performed stereotaxic intra-medullary injection of an AAV2-mCherry vector to transduce either: (1) ipsilateral rVRG neurons or (2) contralateral rVRG neurons. At 7 weeks post-injury, we performed in vivo compound muscle action potential (CMAP) recording separately on each hemidiaphragm to evaluate functional innervation of the diaphragm by PhMNs. At 4 days after CMAP recording, we intrapleurally injected Cholera Toxin B Subunit to selectively label PhMN cell bodies within the cervical spinal cord. At 8 weeks post-injury, we performed in vivo electromyography (EMG) recordings during normal eupnic breathing to assess hemidiaphragm function, and animals were then euthanized for tissue collection.

2.2. LAR peptide promoted recovery of diaphragm function after C2 hemisection SCI

Deficits in inspiratory diaphragm function can result from disruption at a number of possible locations along the rVRG-PhMN-diaphragm neural circuit, including rVRG axon status, rVRG axon-PhMN synaptic connectivity, PhMN health, phrenic axon-diaphragm synaptic connectivity, and diaphragm muscle. In this study, we aimed to determine whether peptide-based LAR inhibition can restore diaphragm function after SCI and, importantly, by which mechanism of circuit plasticity this recovery occurs using a comprehensive set of neuroanatomical and in vivo functional assays.

We first examined diaphragm function by quantitively measuring inspiratory bursting during normal eupnic breathing using in vivo EMG recordings of the hemidiaphragm ipsilateral to the SCI. As rVRG-PhMN disconnection after C2 hemisection results in nearly-complete EMG silencing of the ipsilateral hemidiaphragm, recovery of EMG amplitudes could be driven by LAR peptide-induced rVRG axon regeneration and synaptic reconnection with PhMNs. The diaphragm is a dome-shaped muscle at the base of the lungs, and under intact conditions, it contracts and moves downward allowing the lungs to expand during inspiration; the diaphragm muscle relaxes during expiration. Ventral, medial and dorsal subregions of each hemidiaphragm correspond to innervation from PhMN cell bodies located at C3, C4 or C5 spinal cord, respectively (Laskowski and Sanes, 1987); therefore, conducting EMG recordings separately at each of these diaphragm subregions potentially allows for correlating functional EMG effects with neuroanatomical plasticity at these different spinal cord regions of the PhMN pool.

In the DMSO-only control group, we observed almost-silenced EMG signals at all three subregions of hemi- diaphragm ipsilateral to the hemisection (Fig. 1B), confirming that C2 hemisection disrupts rVRG-PhMN-diaphragm signaling. On the contrary, we observed a significant recovery of diaphragm EMG amplitudes at both ventral and medial sub-regions of ipsilateral hemidiaphragm after treatment with LAR peptide (Fig. 1C). Quantification of

ipsilateral hemidiaphragm EMG amplitudes from each subregion was the following (in μV.s): ventral, 0.7 ± 0.1 for DMSO versus 2.7 ± 0.4 for LAR peptide, $P < 0.001$ (Fig. 1D); medial, 0.6 ± 0.1 for DMSO versus 1.4 ± 0.3 for LAR, $P = 0.03$, (Fig. 1E); dorsal, 0.6 ± 0.1 for DMSO versus 1.0 ± 0.1 for LAR, $P = 0.4$ (Fig. 1F), $n = 8–10$ rats per group for each subregion. We also compared EMG amplitude at all three subregions of hemidiaphragm contralateral to the hemisection and found no differences between DMSO-only and LAR peptide treated groups. Quantification of contralateral hemidiaphragm EMG amplitudes from each subregion was the following (in μV.s): ventral, 8.0 ± 0.4 for DMSO versus 8.8 ± 0.4 for LAR peptide (Fig. 1D); medial, 8.3 ± 0.4 for DMSO versus 8.7 ± 0.4 for LAR (Fig. 1E); dorsal, 9.4 ± 0.3 for DMSO versus 8.2 ± 0.4 for LAR (Fig. 1F), $P > 0.05$ for all contralateral three subregions, one-way ANOVA, $n = 8–10$ rats per group for each subregion. These data from the contralateral hemidiaphragm show both that contralateral hemidiaphragm function was not altered by LAR peptide and that we do not encounter significant animal-to-animal variability in measuring diaphragm EMG amplitude.

Overall, EMG data demonstrate that treatment with LAR peptide promotes ipsilateral hemidiaphragm functional improvement in vivo compared to DMSO-only control. We next sought to mechanistically explore how LAR inhibition is mediating this recovery.

2.3. LAR peptide did not affect functional innervation of the diaphragm by PhMNs

Diaphragm functional deficits after C2 hemisection (as well as LAR peptide experimentally-induced recovery) as reflected by EMG amplitude could be caused by dysfunction at a number of points along the rVRG-PhMN-diaphragm pathway: central drive from rVRG neurons to PhMNs, PhMN drive to diaphragm, or diaphragm muscle fiber activation. We first tested whether hemisection-alone or LAR peptide treatment altered functional innervation of the diaphragm by PhMNs. To do so, we performed in vivo quantitative recordings of CMAP amplitude from the ipsilateral or contralateral hemidiaphragm in response to supramaximal stimulation of the ipsilateral or contralateral phrenic nerve, respectively. Using this approach, we activate all phrenic motor axons and can then measure the post-synaptic depolarization response across all muscle fibers in the hemidiaphragm muscle. Representative traces of ipsilateral or contralateral hemidiaphragm CMAP responses are shown in Fig. 2 (A, B for DMSO-only control group; C, D for LAR peptide group). Quantitative analysis showed no differences in peak CMAP amplitude (Fig. 2E), duration (data not shown) or latency (i.e. time from stimulus to the initial CMAP deflection from baseline; data not shown) between DMSO-only control and LAR peptide groups, including in both the ipsilateral and contralateral diaphragm. The average peak CMAP amplitude ipsilateral to the injury site was 7.2 ± 0.5 mV for DMSO-only and 7.2 ± 0.7 mV for LAR peptide ($n = 4$ per group, $P = 0.87$, one-way ANOVA), while average peak CMAP amplitude contralateral to the hemisection was 6.7 ± 0.6 mV for DMSO and 6.6 ± 0.2 mV for LAR peptide ($n = 4$ per group, $P = 0.88$, one-way ANOVA). These data demonstrate that C2 hemisection did not alter functional innervation of the diaphragm by PhMNs compared to the intact side and that in hemisection animals LAR peptide treatment also did not affect functional diaphragm innervation.

2.4. LAR peptide did not affect morphological innervation of the diaphragm by PhMNs

Previous work from our lab and others demonstrated that cervical contusion-type SCI models that produce damage to PhMN cell bodies within the C3-5 spinal cord result in significant morphological denervation at the diaphragm neuromuscular junction (NMJ) (Nicaise et al., 2013; Nicaise et al., 2012a; Nicaise et al., 2012b), the critical synapse between phrenic motor axons and diaphragm muscle fibers. At eight weeks after injury, we morphologically determined whether NMJ innervation was compromised after C2 hemisection SCI and whether LAR peptide treatment affected this important synapse. Specifically, using whole-mount immunohistochemistry of the muscle, we labeled post-synaptic nicotinic acetylcholine receptors with fluorescently-conjugated alpha-bungarotoxin (red), and we labeled pre-synaptic phrenic motor axons all the way to their terminals with an antibody against neurofilament (SMI-312, green) and a second antibody against synaptic vesicle protein 2 (SV2, also green). As shown in representative confocal z-stacks, nearly all NMJs in the ipsilateral hemidiaphragm were intact in C2 hemisection animals receiving either DMSO-only (Fig. 3A–F) or LAR peptide (Fig. 3G–L). Intact NMJs are characterized by complete apposition of the pre- and post-synaptic labeling. To quantitatively assess this innervation, we identified three primary NMJ morphologies: intact innervation (99.2 ± 0.4% of all NMJs in DMSO-only, $n = 3$ versus 99.5 ± 0.3%, $n = 4$ in LAR peptide; $P > 0.05$ by ANOVA); partial denervation (0.25 ± 0.25% in DMSO, $n = 3$; 0.20 ± 0.20% in LAR peptide, $n = 4$; $P > 0.05$ by ANOVA), in which there is only partial overlap of the motor axon with the post-synaptic receptors; complete denervation (0.0 ± 0.0% in DMSO, $n = 3$ versus 0.0 ± 0.0% in LAR peptide, $n = 4$; $P > 0.05$ by ANOVA). There were no differences in the percentages of intact, partially-denervated or completely-denervated NMJs between rats treated with DMSO-only and LAR peptide (Fig. 3M). In addition, LAR peptide had no effect on the portion of NMJs innervated by multiple phrenic motor axons (0.67 ± 0.34% in DMSO, $n = 3$; 0.25 ± 0.25% in LAR peptide, $n = 4$; $P > 0.05$ by ANOVA) or the percentage of NMJs with thin preterminal axons, a phenotype indicative of denervation and subsequent reinnervation (0.0 ± 0.0% in DMSO, $n = 3$; 0.0 ± 0.0% in LAR peptide, $n = 4$; $P > 0.05$ by ANOVA) (Fig. 3M). These NMJ and CMAP results (i.e. absence of both functional and morphological denervation of the diaphragm by PhMNs on the side of hemisection SCI) were not unexpected given that the SCI was conducted at C2, which is just rostral to the rostral-most-part of the phrenic nucleus. Combined with the CMAP findings, these NMJ data also demonstrate that LAR peptide delivery did not promote functional recovery by affecting PhMN innervation of the diaphragm.

2.5. LAR peptide promoted rVRG axon regeneration through the lesion and into the intact caudal spinal cord

After CNS injury, damaged axons are unable to regenerate in mammals without therapeutic intervention, including rVRG axons (Charsar et al., 2019; Urban et al., 2019a; Urban et al., 2019b). Even with experimental manipulation of axon growth inhibitory mechanisms (especially using non-genetic approaches), it is extremely challenging to achieve long-distance axon regeneration, in particular through the lesion site and back into the distal intact spinal cord where regenerating axons could connect with post-synaptic neuronal targets. To determine whether LAR peptide treatment promoted rVRG axon regeneration, we selectively labeled only rVRG axons by transducing rVRG neurons within the medulla

ipsilateral to the hemisection with AAV2-mCherry (Fig. 4A). To determine whether our AAV2-mCherry labeling strategy was consistent across animals both within and across groups, we quantified the number of transduced rVRG cell bodies in the medulla. There was no difference in the number of AAV2-mCherry transduced rVRG neuron cell bodies between the two experimental groups (DMSO: 19 ± 2 rVRG neurons per section; LAR: 24 ± 5, $P = 0.32$, *t*-test, $n = 4$ rats per group, Fig. 4C–E).

To histologically verify lesion completeness before performing rVRG axon regeneration analysis, we performed both GFAP immunostaining (Fig. 4F–H) and and cresyl violet staining (data not shown) on cervical spinal cord sections from DMSO-only and LAR peptide rats. We found that the C2 hemisection was anatomically complete in every rat. In a separate cohort of rats receiving C2 hemisection-only (but no LAR peptide or DMSO-only treatment), we observed silencing of ipsilateral hemidiaphragm EMG activity at two weeks post-injury (i.e. a time point before the small amount of spontaneous ipsilateral EMG recovery occurs in the C2 hemisection model) in all tested animals ($n = 5$ rats; data not shown), further supporting the completeness of our lesion. While these EMG recordings at 2 weeks post-injury were not conducted in the injured rats receiving LAR peptide or DMSO-only, these data nevertheless support the consistent completeness of our C2 hemisection surgical procedure.

In addition, we quantified lesion size to determine whether LAR peptide treatment impacted the histological extent of spinal cord damage compared to the DMSO-only control group, which could contribute to LAR peptide-induced functional recovery. To measure lesion size, we performed GFAP immunohistochemistry on sagittal spinal cord sections to identify the border between intact tissue and lesion. We quantified rostral-caudal distance from the rostral to caudal borders of the lesion and found no difference between the experimental groups (Fig. 4F–H): 393.8 ± 59.6 μm in DMSO-only group; 362.8 ± 36.6 μm in LAR peptide group, $P = 0.67$, *t*-test, $n = 4$ rats per group. These data suggest that a neuroprotective effect of LAR peptide was not involved in the observed functional diaphragm recovery.

Transduction of the rVRG neuronal cell bodies resulted in anterograde labeling of rVRG axons within the cervical spinal cord. Sagittal spinal cord sections from animals with ipsilateral rVRG labeling were triple immunostained with DsRed (to enhance mCherry signal), vesicular glutamate transporter 2 (VGLUT2) to label excitatory presynaptic terminals (as rVRG neurons are glutamatergic) and CTB (to selectively label PhMN cell bodies). CTB-labeled PhMNs were continuously distributed in a column within the ventral grey matter extending along levels C3 to C5 (Fig. 5A). rVRG axon regeneration was quantified as the number of mCherry tracer-labeled rVRG axons at different distances rostral to the lesion site, within the lesion, and in the caudal intact spinal cord (Fig. 5A).

Both DMSO-only and LAR peptide treated animals showed rVRG axons rostral to the lesion (Fig. 5B,E). However, in the DMSO-only group, no rVRG axons were observed regrowing into or through the lesion (Fig. 5C) or into the caudal spinal cord (Fig. 5D), consistent with the results of our previous studies with untreated C2 hemisection-only conditions (Charsar et al., 2019; Urban et al., 2019a). In the LAR peptide group, we observed significant growth of

rVRG axons across the rostral intact-lesion interface, across the lesion site and across the caudal lesion-intact interface (Fig. 5F), and finally for several segments along the intact caudal spinal cord (Fig. 5G). Quantification of mCherry$^+$ axon regrowth profiles at different rostral-caudal distances (Fig. 5H) shows that LAR peptide was effective at stimulating rVRG axon regeneration across an anatomically-complete SCI lesion, with these axons even reaching the C3 (corresponding to 1500 μm bar in Fig. 5H), C4 (corresponding to 3000 μm bar in Fig. 5H) and C5 (corresponding to 4500 μm bar in Fig. 5H) spinal cord segments (asterisk indicates $P < 0.05$, ANOVA, $n = 4$ per group). Furthermore, to explore the relationship between rVRG axon regeneration and functional EMG improvement induced by LAR peptide, we examined the correlation between the degree of rVRG axon regeneration at the C3 level and EMG amplitude in the corresponding ventral diaphragm subregion (Fig. 5I). There was a correlation between these two outcomes in the LAR peptide group (correlation coefficient for linear fit, $R^2 = 0.98$, $P = 0.01$); data from DMSO-only control were not included in this analysis as absolutely no rVRG axon regeneration was observed in this group. These findings suggest that regeneration of rVRG axons across the lesion and into the intact caudal spinal cord (i.e. the location of the PhMN pool) was at least in part responsible for the recovery of diaphragm function induced by LAR peptide.

2.6. LAR peptide promoted putative monosynaptic connection between regenerating rVRG axon and PhMNs

Achieving long-distance axon regeneration following SCI is a major challenge. In addition to this axonal regrowth, it is also critical for these axons to synaptically connect with appropriate neuronal targets to promote recovery of function. This synaptic integration can include connectivity with the original post-synaptic targets of the axotomized neurons and/or generation of circuitry via novel connections. To investigate whether regenerating ipsilateral-originating rVRG axons formed synaptic connections with PhMNs on the side of hemisection SCI, we assessed the number of putative synaptic connections specifically between mCherry/DsRed-positive rVRG fibers and CTB-labeled PhMN cell bodies at level C3 using confocal acquisition of z-stacks and quantification of rVRG axon-PhMN contacts using single-Z section analysis to establish direct apposition of pre-synaptic VGLUT2$^+$/mCherry$^+$ axon terminals and post-synaptic CTB$^+$ PhMNs. We observed no putative rVRG-PhMN synapses in the DMSO-only control (Fig. 6A–D), as expected since no rVRG axon regeneration was achieved in this group. On the contrary, we observed large numbers of putative rVRG-PhMN synapses in the LAR peptide group (Fig. 6E–H). We quantified the number of these synaptic connections per individual PhMN at C3 and then plotted these data against the EMG amplitude results from the corresponding ventral subregion (Fig 6I); there was strong correlation between these datasets (.$R^2 = 0.99$; $P < 0.0001$), further supporting the notion that rVRG axon regeneration and rVRG-PhMN circuit reconnectivity at least in part was responsible for LAR peptide-induced functional recovery. In addition to putative excitatory synapses between mCherry$^+$ rVRG axons and PhMNs, we also quantified the effects of LAR peptide on excitatory synapses from mCherry$^-$/VGLUT2$^+$ non-rVRG inputs on ipsilateral CTB$^+$ PhMNs at C3: 11.8 ± 0.9 putative mCherry$^-$/VGLUT2$^+$ excitatory synapses per CTB$^+$ PhMN in DMSO-only group; 16.4 ± 1.9 in LAR treated group, $P = 0.07$, t-test, $n = 4$ rats per group, Fig 6J). While not significant, the trend toward an increase suggests that LAR peptide may also enhance excitatory synaptic input to PhMNs from other

neuronal populations in addition to rVRG axons (e.g. possibly from excitatory interneurons, sensory afferents, and various projection neuron populations originating in supraspinal locations other than rVRG).

2.7. LAR peptide promoted sprouting of rVRG axons within the PhMN pool

Axon sprouting, defined as fine nerve processes or "sprouts" that grow out from injured or spared axons, has long been considered an important form of plasticity that can drive recovery of function both spontaneously and in response to therapeutic intervention following CNS damage (Meves and Zheng, 2014). We examined whether sprouting of spared rVRG axons originating in the contralateral medulla was induced by LAR peptide by injecting the AAV2-mCherry anterograde tracer into the contralateral rVRG and then quantifying sprouting of these axons within the PhMN pool on the side of the hemisection (i.e. contralateral to the location of their cell bodies) (Fig. 4B). Sagittal spinal cord sections were double-immunolabeled with DsRed and CTB. We then counted numbers of $mCherry^+$ fibers within the phrenic nucleus (i. e. the location of CTB^+ PhMNs) at distances of 1.5 mm, 3.0 mm and 4.5 mm caudal to the lesion that correspond to C3, C4 and C5 levels, respectively (Fig. 7A). Representative confocal images show PhMNs labeled with CTB that were surrounded by contralateral-originating $mCherry^+$ rVRG axons (Fig. 7B–G). We observed that these contralateral-originating rVRG axons are present within the PhMN pool on the side of hemisection even in the DMSO-only condition (Fig. 7D, H). The average number of these $mCherry^+$ fibers in the LAR peptide group (11.8 ± 0.6, $n = 5$) increased significantly ($P < 0.001$, one-way ANOVA analysis, Fig. 7E–G, 7I, 7K) compared to DMSO-only control (3.4 ± 0.8, $n = 5$) at C3 (Fig. 7B–D, 7H, 7K) and C4 (2.7 ± 0.3 in DMSO, $n = 5$; 8.7 ± 1.3 in LAR peptide, $n = 5$; $P = 0.002$, one-way ANOVA, Fig. 7L), but there was no statistical significance in the difference at C5 (3.2 ± 0.8 in DMSO, $n = 5$ versus 7.1 ± 1.5 in LAR peptide, $n = 5$; $P = 0.052$, one-way ANOVA, Fig 7M). We next examined whether there was a relationship between this sprouting and diaphragm functional recovery by assessing the correlation between the degree of rVRG axon sprouting at the C3 level and EMG amplitude in the corresponding ventral diaphragm subregion (Fig. 7J). Unlike with the correlation between rVRG axon regeneration and EMG amplitude (Fig. 6I), we found no correlation between rVRG axon sprouting and diaphragm recovery ($R^2 = 0.75$; $P = 0.14$).

2.8. LAR peptide promoted sprouting of modulatory serotonergic axons within the PhMN pool

Modulatory serotonergic axons whose cell bodies reside in one of several raphe nuclei of the brain play an important role in regulating the excitability of neuron populations across the CNS, in particular spinal cord lower motor neurons such as PhMNs (Fisher et al., 2011). Furthermore, plasticity of this serotonergic input has been shown to be involved in recovery of diaphragm function after cervical SCI, including both in the absence and presence of therapeutic intervention (Goshgarian, 2003; Perrin and Noristani, 2019). At 8 weeks post-injury, we assessed the density of serotonergic axon innervation within the PhMN pool by performing immunohistochemistry for serotonin (5-HT) and quantifying the total length of 5-HT+ axons. Compared to DMSO-only control (Fig. 8A–B), LAR peptide significantly increased the total 5-HT axon length within the phrenic nucleus at C3 (Fig. 8B–C) (3376 ± 779 μm in DMSO versus 8473 ± 1562 μm in LAR peptide, $n = 6$ per group animals, $P =$

0.02, one-way ANOVA). However, LAR peptide did not affect the density of 5-HT axon innervation of the PhMN pool at C4 (5135 ± 1861 in DMSO; 6952 ± 1501 in LAR peptide, $n = 6$ per group animals, $P = 0.42$, one-way ANOVA; Fig. 8D) or C5 (4973 ± 2109 in DMSO; 6657 ± 1461 in LAR peptide, $n = 6$ per group animals, $P = 0.44$, one-way ANOVA; Fig. 8E).

3. Discussion

3.1. Long-distance regeneration versus sprouting

We find that LAR peptide administration resulted in both regeneration of injured rVRG axons and sprouting of spared rVRG and serotonergic axons. Our results are not in line with the body of work suggesting that modulating CSPG-mediated axon growth inhibition stimulates local sprouting and synaptic rearrangement but not long-distance regeneration (reviewed in (Sofroniew, 2018)), though other studies have shown the axon regeneration promoting effects of targeting CSPGs after CNS injury (Bradbury et al., 2002). The current work and our previous studies (Urban et al., 2019b) demonstrate that rVRG axons are robust regenerators in response to targeting of growth inhibitory mechanisms; therefore, one possible explanation may be that the axon growth phenotype (i.e. regeneration versus sprouting) may differ with the specific axon population being examined. Interestingly, our previous work with a PTPσ inhibitory peptide showed functional diaphragm recovery in the C2 hemisection model (employing the same peptide delivery approach as we used for LAR peptide), but no regeneration of rVRG axons; instead, we found only sprouting of spared rVRG axons within the ipsilateral PhMN pool in response to PTPσ peptide (Urban et al., 2019a). These differences in the plasticity of rVRG-PhMN circuitry between LAR and PTPσ peptides may be explained by the findings that PTPσ and LAR can signal in part through non-overlapping intracellular transduction pathways that may be regulating different axon growth responses (Ohtake et al., 2016). Furthermore, our current and previous data collectively provide rationale for the combination of both PTPσ and LAR inhibition to maximize recovery via the simultaneous modulation of multiple signaling pathways and consequently multiple forms of axon growth (Ohtake et al., 2016).

Using our analysis of only 40 μm thick spinal cord sections, we are not tracking regeneration of individual rVRG axons over long distances; therefore, caution is needed in making the conclusion that LAR peptide promoted regeneration of injured rVRG axons across the lesion site and back into the caudal intact C3-C5 spinal cord. However, we do clearly observe in every LAR-treated animal individual rVRG axons growing across the rostral intact-lesion interface into the lesion site, and we similarly observe in every LAR-treated animal individual rVRG axons growing across the caudal lesion-intact interface back into the caudal intact spinal cord. Furthermore, we never observe this in any animal in the DMSO-only control group. Therefore, while we have not followed individual axons along this entire journey, the data strongly suggest that they regenerated through the lesion.

Findings in the field suggest that there is some double-crossed rVRG input to the PhMN pool originating in the ipsilateral rVRG (i.e. rVRG axons cross and then re-cross back as they descend from the medulla to the phrenic nucleus) (Boulenguez et al., 2007). Interestingly, we observed absolutely no ipsilateral-originating rVRG axon labeling within

the PhMN pool ipsilateral to the hemisection in the DMSO-only control group, suggesting that the ipsilateral-originating rVRG axons that we observe at this location in the LAR peptide group made it there by growing through (and/or around) the lesion. This is supported by our observations of ipsilateral-originating rVRG axons growing into the lesion, across the lesion, and back out of the lesion into the distal/caudal spinal cord (even if we have not tracked single axons along this entire journey). Alternative explanations are possible, including that some of these ipsilateral-originating rVRG axons (that we observe in the ispilateral PhMN pool in response to LAR peptide) are normally located in the contralateral cervical spinal cord and that LAR inhibition caused them to sprout across the spinal cord to reach the ipsilateral PhMN pool. This would not explain the lack of these ipsilateral-originating rVRG axons in the ipsilateral PhMN pool in the DMSO-only condition in the context of “double-crossing”, as we would expect to see them there even in the absence of therapeutic manipulation. It is possible that multiple plasticity mechanisms are occurring; nevertheless, our data strongly suggest that regeneration of injured ipsilateral-originating rVRG axons was significantly involved in the observation of these axons in the ipsilateral PhMN pool caudal to the hemisection.

3.2. Mechanism of axon growth driving functional recovery

In this study, we sought to determine which axon growth mechanism (s) stimulated functional diaphragm recovery in response to LAR peptide. It is particularly challenging to determine the mode(s) of circuit plasticity causally responsible for recovery of function in an in vivo model of SCI. Along these lines, we have not definitively determined whether regeneration, sprouting or a combination of both drove diaphragm recovery, though we do provide a large amount of functional and neuroanatomical data that shed significant light on this important question.

We observe significant regeneration of injured rVRG axons into and through the lesion site and, importantly, back into the distal intact spinal cord where they reach the cell bodies of the PhMNs ipsilateral to the hemisection. Interestingly, we find that this rVRG axon regeneration was the most robust at the C3 and C4 levels, with significantly less regeneration at the more caudal C5 segment (Fig. 5H). Correspondingly, we find diaphragm recovery with our EMG recordings only at the ventral and medial subregions of the muscle that are innervated by PhMNs primarily located at C3 and C4, respectively, but not at the dorsal subregion that is controlled by C5 PhMNs (F 1 D-F). In addition, we find that there is some degree of animal-to-animal variability in both EMG recovery and rVRG axon regeneration in response to LAR peptide and that this recovery is strongly correlated with the amount of rVRG axon regeneration (Fig. 5I). Similarly, EMG recovery correlated with the degree of rVRG-PhMN monosynaptic connections within the ipsilateral spinal cord (Fig. 6I). Collectively, these data suggest that rVRG axon regeneration was possibly responsible - at least in part - for driving functional diaphragm recovery.

In our published work with a PTEN antagonist peptide, we also found robust rVRG axon regeneration and diaphragm recovery in the C2 hemisection model (Urban et al., 2019b). In this previous study, we found that re-lesion through the hemisection site completely ablated recovery, demonstrating that regeneration through the injury site was causally responsible

specifically for PTEN inhibition-induced improvement and more generally that long-distance axon regeneration is a growth mechanism that can lead to diaphragmatic recovery after SCI (which has also been shown by Alilain and colleagues (Alilain et al., 2011). We did not perform a similar re-lesion experiment in the current study with LAR peptide, leaving the possibility open that input from the spared contralateral spinal cord was the key mechanism (or that the combination of input from both the ipsilateral and contralateral sides together promoted functional improvement). To this point, we found significant sprouting within the ipsilateral PhMN pool of spared rVRG axons originating in the contralateral rVRG (Fig. 7). This finding is in line with a number of studies that have shown that CSPG modulation in the injured CNS promotes local sprouting (Sofroniew, 2018). Furthermore, sprouting of spared circuitry is an important plasticity mechanism that has been shown to promote functional recovery in SCI models both spontaneously and in response to therapeutic interventions (Bareyre et al., 2004). Importantly, achieving long-distance axon regeneration and reconnection of original circuitry is not necessary for promoting recovery after SCI. In the context of respiratory neural circuitry, spared contralateral-originating rVRG input plays a central role in the small amount of diaphragm recovery that occurs after C2 hemisection SCI, both spontaneously and in response to various manipulations (Goshgarian, 2003). Enhancing this spared input to the phrenic nucleus is a potentially powerful approach for stimulating respiratory recovery post-SCI. Interestingly, we observed rVRG axon sprouting at C3 and C4, but not at C5, which corresponds to the pattern of EMG recovery at two of the three diaphragm subregions. However, we did not find a correlation between the degree of rVRG axon sprouting and EMG amplitude (Fig. 7J), suggesting that this plasticity mechanism may not have played a role in recovery (or played a lesser role than rVRG axon regeneration). In another of our previous studies, we found in the C2 hemisection model that PTPσ inhibitory peptide promoted recovery of diaphragm function in the absence of any rVRG axon regeneration (Urban et al., 2019a). Instead, PTPσ peptide stimulated robust sprouting of rVRG axons within the ipsilateral phrenic nucleus, and we observed that re-lesion through the hemsiection site had no effect on diaphragm recovery, demonstrating that functional efficacy was based primarily on input from the spared contralateral spinal cord after PTPσ inhibition.

Furthermore, we observed serotonergic axon sprouting within the ipsilateral phrenic nucleus at C3, but not at C4 or C5. These data may suggest that the combination of the highest level of rVRG axon regeneration in the C3 spinal cord plus 5-HT axon sprouting at this same location together produced the most significant EMG recovery in the ventral diaphragm subregion, which is in line with the modulatory effect of serotonergic input on glutamatergic neurotransmission in spinal motor neurons (Dale-Nagle et al., 2010). Functional recovery was also noted in the medial diaphragm; however, this recovety was not as robust as in the ventral diaphragm, and it was accompanied by lesser rVRG axon regeneration to the C4 spinal cord and an absence of 5-HT axon sprouting within the C4 portion of the ipsilateral PhMN pool. It is surprising that we found increased density of 5-HT axons within the C3, but not C4 or C5 PhMN pool, if this effect was due to a sprouting response. Instead, we would expect to see equivalent 5-HT axon sprouting across the phrenic nucleus. A possible explanation is that the greater density of 5-HT axons at C3 is due instead to regeneration of 5-HT axons across the lesion site, with these axons first reaching C3 and then not extending

farther in the caudal direction. A number of studies have demonstrated growth of serotonergic axons in response to manipulation of CSPG signaling after SCI. For example, Lang and colleagues showed that delivery of a PTPσ inhibitory peptide stimulates significant 5-HT axon growth caudal to the thoracic SCI site, as well as recovery of bladder function (Lang et al., 2015). In the context of damaged respiratory circuitry, we have shown that PTEN antagonist peptide (Urban et al., 2019b), PTPσ inhibitory peptide (Urban et al., 2019a), BDNF-releasing hydrogel (Ghosh et al., 2018) and intraspinal injection of an AAV2-BDNF vector (Charsar et al., 2019) each can promote 5-HT axon sprouting within the PhMN pool in C2 hemisection and mid-cervical contusion models of SCI. Warren and colleagues also showed that Chondroitinase ABC delivery can promote significant serotonergic axon growth and diaphragm recovery in the chronically injured cervical spinal cord (Warren et al., 2018). Collectively, our studies and the work of others in the field suggest that plasticity of serotonergic input to PhMNs is an important mechanism for stimulating diaphragmatic recovery after SCI and that targeting CSPG signaling via LAR and PTPσ manipulation is a promising approach for achieving this goal.

An intriguing possibility is that different circuit plasticity mechanisms were responsible for driving recovery at different portions of the PhMN pool in response to LAR inhibition. Going forward, it will be important to utilize experimental approaches such as selective silencing of specific neuronal populations using techniques like chemogenetics (Roth, 2016) to explore this issue more comprehensively and with greater experimental precision.

Another possible explanation for our observation of functional recovery at the ventral and medial (but no dorsal) muscle subregions could be due to a LAR peptide gradient, with the highest peptide levels closest to the site of gelfoam delivery at C2 and progressively decreasing levels at more caudal locations along the PhMN pool contributing (completely or in part) to the differential functional effects observed across the three muscle sub-regions. Moving forward, we could begin to explore this idea by measuring peptide levels at different neuroanatomical locations.

3.3. Synaptic connections

The improvement of diaphragm function with LAR peptide could have been due to direct effects on synaptic rearrangement instead of (or in addition to) axon growth responses. Such synaptic effects could modulate the input from spared and/or regenerating axon populations. Previous work has shown that RPTPs such as LAR and PTPσ play an important role in synaptic development, in particular of excitatory synapses (Takahashi and Craig, 2013; Um and Ko, 2013). In this study, we find significant numbers of putative monosynaptic connections between regenerating rVRG axons and PhMN somata across the phrenic nucleus. As we observe absolutely none of these putative synapses in the DMSO-only control condition, the generation of these synapses may have been due just to LAR peptide promoting rVRG axon regeneration, with some of these regenerating axons making connections with PhMNs because of proximity and not because LAR inhibition directly enhanced synaptogenesis. We did not quantify monosynaptic connections between contralateral-originating rVRG axons and PhMNs in our study; going forward, this could be a useful approach to explore this question as we could control for the density of rVRG axons

surrounding the PhMN somata and thereby assess LAR peptide's effects specifically on levels of synapse formation independent of sprouting.

3.4. Immune cell response

Development and function of the immune system is regulated by RPTPs such as LAR and PTPσ (Pike and Tremblay, 2013). Furthermore, intraspinal inflammatory cell responses after SCI affect axon growth processes such as dieback and regrowth (Silver et al., 2014). Therefore, it is possible that LAR peptide indirectly impacted rVRG and serotonergic axon growth via primary effects on inflammatory processes within the lesion and in the surrounding intact spinal cord. Interestingly, PTPσ genetic knockout or peptide-based inhibition worsen autoimmune responses in a mouse model of multiple sclerosis (Ohtake et al., 2017), suggesting that LAR inhibition could worsen outcome after cervical SCI by magnifying the proinflammatory response and therefore not produce the beneficial effects we observe in the current study. However, like other biological processes regulated by proteoglycan signaling, the effects of RPTP activation depend on the specific receptor (e.g. LAR versus PTPσ effects can differ). In addition, the immune cell effects of signaling can vary depending on whether the ligand is CSPG or another proteoglycan such as HSPG that can produce in some cases drastically different biological outcomes (Ohtake et al., 2018). Relative to PTPσ, little is known about the role of LAR in immune cell function (Kondo et al., 2010; Terszowski et al., 2001), particularly in the context of nervous system pathophysiology. Future work will be needed to explore the contribution of immune cell modulation to LAR peptide effects after SCI.

3.5. Source of CSPGs acting on LAR

Findings in the field are beginning to suggest that a major portion of the axon growth-inhibitory CSPGs is not provided by reactive astrocytes around the lesion, but instead by non-astrocyte sources such as other scar-forming cell types (Anderson et al., 2016; Cregg et al., 2014). Importantly, an ongoing body of work (Smith et al., 1986; Smith et al., 1987; Smith et al., 1990; Smith and Silver, 1988), including exciting recent studies (Anderson et al., 2016), suggests that astrocytes are axon growth-promoting, contrary to long-established beliefs. Astrocyte-mediated mechanisms that may be capable of promoting regeneration of damaged axons and sprouting of spared fibers include: (1) providing a cellular substrate for axon extension in the cystic lesion; (2) provision of beneficial molecules such as neurotrophins (Davies et al., 2006; Haas et al., 2012; Hamby and Sofroniew, 2010; Hill et al., 2004); (3) production of extracellular matrix and cell adhesion molecules (Falnikar et al., 2015); and (4) immunomodulation (Sofroniew, 2015). Furthermore, therapeutic approaches aimed at enhancing the presence of pro-regenerative astrocytes using strategies such as transplantation of astrocyte progenitors or differentiated astrocytes have shown success in promoting axon growth in animal models of CNS trauma, including SCI (Davies et al., 2006; Davies et al., 2008; Haas and Fischer, 2013; Haas et al., 2012; Shih et al., 2014; Smith et al., 1986; Smith et al., 1987; Smith et al., 1990; Smith and Silver, 1988).

3.6. Conclusions and future directions

Excitingly, we have shown that inhibition of LAR via a peptide-based approach results in significant recovery of diaphragm function, relatively long-distance regeneration of

descending respiratory axon populations and partial reconnection of damaged rVRG-PhMN-diaphragm circuitry in a severe model of high-cervical SCI. Moving forward, it will be important to extend this work to test delivery at a more delayed time point post-injury, including in a chronic SCI model given the large population of individuals that are chronically injured (Ahuja et al., 2017). In this study, we employed a relatively-invasive peptide delivery approach involving surgical placement of the soaked gelfoam on the dorsal surface of the spinal cord. It will be critical to determine whether we can also achieve similar therapeutic efficacy with less-invasive methods such as systemic or intrathecal delivery (Urban et al., 2019b). We have previously shown that systemic delivery of PTEN antagonist peptide can promote diaphragm recovery in this same hemisection model (Urban et al., 2019b), suggesting that a similar approach with our LAR peptide may be feasible. In this study, we restricted our approach to only a single peptide dosing and duration paradigm. It will be interesting to determine whether we can enhance therapeutic effects with a modified peptide delivery protocol. In addition to LAR peptide, there exist a number of possible approaches to modulate CSPG signaling such as enzymatic GAG side chain removal from CSPGs (Bradbury et al., 2002), antibody-based (Wu et al., 2017) or small molecule (Keough et al., 2016) targeting of LAR and PTPσ, and modulation of other RPTPs besides LAR such as PTPσ (Urban et al., 2019a). It will be interesting moving forward to compare the therapeutic efficacy, potential side effects and various practical advantages and disadvantages of these different approaches in cervical SCI models and specifically on respiratory improvement. Finally, it is unlikely that LAR inhibition alone will be sufficient for achieving maximal functional recovery. Our current work demonstrates the therapeutic power of this novel LAR peptide approach and also provides extensive data suggesting the plasticity mechanisms by which LAR inhibition can affect respiratory neural circuitry. Going forward, it will be important to test the combination of LAR peptide with other strategies targeting axon growth inhibitory and promoting mechanisms, as well as interventions such as rehabilitative training regimens (Fuller and Mitchell, 2017), to promote additive - or even synergistic - therapeutic effects on respiratory function following SCI.

3.7. Experimental procedures

3.7.1. Animals—Adult female Sprague-Dawley rats weighing 250–350 g from ENVIGO (formally Harlan Laboratories) were used in this study. Male animals were not used in this study. Rats were housed in a controlled environment (12 h light/dark cycles) with food and water ad libitum. All experimental procedures involving animals were performed under the approval of the Institutional Animal Care and Use Committee (IACUC) of the Thomas Jefferson University. Animal surgeries and pre- and postsurgical care were performed in compliance with ARRIVE (*Animal Research: Reporting of* In Vivo *Experiments*) Guidelines for the Care and Use of Laboratory Animals. Prior to surgery, animals were randomly assigned into the following groups: DMSO-only vehicle control or LAR peptide. All surgeries and subsequent functional and histological analyses were always performed in a blinded manner. DMSO-only treated animals served as vehicle controls and were subjected to the same procedures as the LAR peptide animals, with the only exception that the LAR peptide was not administered.

3.7.2. Spinal cord injury (SCI) and postoperative care—Anesthesia was induced with xylazine (10 mg/kg, s.q.) (Akorn Inc., Lake Forest, Illinois) and ketamine (120 mg/kg, i.p.) (Vedco, Saint Joseph, Missouri). The skin overlying the dorsal side of spinal cord was shaved and disinfected (betadine and 70% ethanol wipes) before surgery. A midline longitudinal incision was made from the base of the skull to the shoulder blades through the skin and muscle overlying the cervical vertebrae. A laminectomy was performed to expose the C2 spinal cord and a right C2 hemisection was performed caudal to the C2 rootlets from the midline to lateral edge of the spinal cord using a micro-scalpel (Urban et al., 2018). To ensure a complete hemisection, a 30-gauge needle (BD Biosciences, San Jose, California) was passed through the lesion several times. Following complete hemisection, the overlying muscles were sutured with sterile 4–0 Vicryl suture, and the skin was closed with sterile wound clips (Braintree Scientific, Braintree, Massachusetts). Rats were given antisedan (1.2 mg/kg, s.q.) (Zoetis, Parsippany-Troy Hills, New Jersey), lactated Ringer's solution (10 ml, s. q.) and buprenorphine (0.01 mg/kg, s.q.) (Patterson Veterinary, Greeley, Colorado) immediately after surgery. Rats were then placed in a clean cage on a surgical heating pad set to 37 °C (Gaymar, Orchard Park, New York) continuously for 5 days. Lactated Ringer's solution (30 ml/day, s.q.) and oral Nutri-cal supplements (1–3 ml/day, Vetoquinol USA Inc., Fort Worth, Texas) were provided until adequate normal eating and drinking resumed. Signs of pain/distress, respiratory distress and infections were closely monitored postoperatively.

3.7.3. LAR peptide treatment—LAR peptide was synthesized commercially with C-terminal amidation by CHI Scientific, and peptide purity was analyzed by mass spectrometry. The peptide sequence was published previously (Fisher et al., 2011). Lyophilized peptide was dissolved in DMSO and then diluted to the final concentration (15 mg/ml) in sterile calcium-free Hanks' balanced salt solution. LAR peptide or DMSO-only vehicle were soaked in gel foam (3.0 mm length x 3.0 mm width x 2.5 mm depth in size) and placed directly over the lesioned spinal cord (50 μl/rat), both immediately after hemisection and again at 7 days post-injury. With respect to the experimental design of peptide delivery, we based this on both our preliminary experiments and practical considerations. However, it is important to point out that it is impossible to identify the perfect delivery paradigm. We choose to deliver the peptide with the soaked gelfoam approach, and we replaced the gelfoam with a fresh piece of soaked gelfoam only once at 7 days post-injury. We chose not to replace the gelfoam additional times for more prolonged delivery because each replacement involves an invasive spinal surgery. Therefore, our paradigm was a balance of practicality and maximizing duration and dosing of delivery. We have shown that delivery of PTPσ peptide with this same gelfoam method promotes significant recovery of diaphragm function in C2 hemisection SCI rats (Urban et al., 2020). We waited until 8 weeks post-injury to perform functional analysis and to sacrifice the animals to provide sufficient time for axon growth and synaptic connectivity. A number of studies reported that SCI rodents maintain functional recovery after terminating peptide-based treatments that promote axon growth (Fisher et al., 2011; Lang et al., 2015; Li and Strittmatter, 2003). It is possible that we would observe similar functional and histological efficacy if animals were sacrificed at an earlier time point; however, we chose only the later time point for this study.

3.7.4. Rostral ventral respiratory group (rVRG) injection—We used adeno associated virus (AAV) serotype 2 driving expression of red fluorescent protein (AAV2-mCherry) to examine the distribution of bulbospinal rVRG projections to the phrenic motor nucleus (Urban et al., 2018). Rats were anesthetized with a mixture of ketamine/xylazine. The head of each rat was fixed in a stereotaxic frame (David Kopf Instruments, Tujunga, CA) with the mouthpiece set at —11 mm below the interaural line. The atlanto-occipital membrane was incised, and the lower aspect of the occipital plate was removed to allow penetration of the injection needle. Focal pressure injections of AAV2-mCherry (medulla; titer: 1.66 × 10e13 vg/ml; volume: 0.3 μl controlled by Micro4 Microsyringe Pump) were targeted to the medullary rVRG located at the following coordinates: 2.0 mm lateral, 1.0 mm rostral, and 2.6 mm ventral from calamus scriptorius, as determined in separate neurophysiological findings (Bezdudnaya et al., 2017; Zheng et al., 1998). In animals receiving C2 hemisection, brainstem and spinal cord tissues were harvested 4 weeks following AAV injection.

3.7.5. Retrograde labeling of phrenic motor neurons (PhMNs)—PhMNs were retrogradely and bilaterally labeled 3 days prior to tissue harvest (Li et al., 2014). Animals were induced with 3% isoflurane in 100% O2, and rats were transferred to a pad and anesthesia was maintained through a nose cone with 1.5–2% isoflurane. While stabilizing the animal's back, the rib cage was palpated in order to identify the fifth intercostal space at the anterior axillary line. Using sterile conditions and appropriate antisepsis, a 50-μ1 Hamilton syringe was used to inject 15–20 μl of a 0.25% Cholera Toxin B Subunit (CTB, Choleragenoid) from Vibrio cholera (List Biological Labs). Injections were performed transcutaneously into the intrapleural space on each side (5–7 mm deep, from skin). Animals were monitored closely for any signs of respiratory deficits such as that following unintentional pneumothorax, but none were evident in all animals in this study.

3.7.6. Electromyography (EMG) recordings and analysis—All animals were anesthetized with xylazine (10 mg/kg, s.q.) and ketamine (120 mg/kg, i.p.). The skin overlying the abdomen was shaved, and an incision was made to expose the right and left hemidiaphragm. Bipolar electrodes spaced 3 mm apart were placed for recording in three separate sub-regions of the hemidiaphragm: dorsal, medial, and ventral. EMG activity (10,000 samples/s) was amplified and filtered through a band-pass filter (50–3000 Hz) by using a PowerLab 8/30 data acquisition system (AD Instruments, Colorado Springs, Colorado) (Li et al., 2015a). Recordings were made separately in each subregion from each animal. Diaphragm EMG traces were rectified and integrated (time constant decay 0.05 s) using LabChart 7 software (AD Instruments, Colorado Springs, Colorado). For each muscle sub-region in an animal, diaphragm output was determined by averaging integrated signal across all inspiratory bursts from three 30-s intervals (30-s intervals were selected that had no sighs) over the total five-minute recording time.

3.7.7. Compound muscle action potential (CMAP) recordings—Phrenic nerve stimulation and CMAP recordings were performed with ADI Powerlab 8/30stimulator and BioAMPamplifier (ADInstruments) (Li et al., 2015b). Rats were anesthetized with isoflurane (Piramal Healthcare, Bethlehem, Pennsylvania) at a concentration of 2.5–3.0%

diluted in oxygen. Rats lay supine and a ground electrode was placed subcutaneously into tail. Recording was obtained from the unilateral costal margin via standard surface electrode. The reference electrode was placed subcutaneously into the contralateral lower abdominal region. The single stimulus duration was set to 0.5 milliseconds duration at 6 mV (amplitude). Stimulating electrodes were placed transcutaneously approximately 1.0 cm deep, 0.5 cm apart, lateral to the trachea and superior to the clavicle. After the single supramaximal stimulation, repetitive nerve stimulation (~ 10 times), with the recording and stimulating electrodes in the same positions, was applied to obtain the average response. A supramaximal CMAP was obtained, and the amplitude was measured from baseline to peak.

3.7.8. Diaphragm whole-mount histological neuromuscular junction (NMJ) analysis—For microscopic examination of whole-mount diaphragm, the diaphragm was dissected, rinsed in PBS (pH 7.4) and fixed in 4% paraformaldehyde (PFA) in PBS at room temperature for 20 min. After the removal of connective tissue, the whole-mount diaphragm was incubated in 0.1 M glycine for 30 min at room temperature. The postsynaptic nicotinic acetylcholine receptors in the diaphragm were labeled with α-Bungarotoxin, Alexa Fluor 555 conjugate (1:200, Invitrogen) at room temperature for 15 min. After washing, the whole-mount diaphragm was permeabilized with ice-cold methanol for 5 min, and then were blocked for 1 h at room temperature in a Trition-BSA-PBS solution composed of 2% bovine serum albumin and 0.2% Triton X-100 diluted in PBS. The diaphragms were incubated with presynaptic vesicle marker anti-SV2 antibody (1:10, Developmental Studies Hybridoma Bank) and neurofilament marker anti-SMI-312 antibody (1:1000, Covance) at 4 °C overnight. After washing with TBP solution, the diaphragms were incubated with Fluorescein (FITC) AffiniPure IgG, Feγ subclass 1 specific secondary antibody (Jackson ImmunoResearch Laboratories) for 1 h at room temperature. Diaphragms were mounted with Vectashield mounting medium (Vector Laboratories), coverslipped and stored at —20 °C. Two blinded researchers quantified the whole-mount diaphragms under a Leica fluorescence microscope. Total numbers of NMJs and percentages of intact, partially-denervated or completely denervated NMJs were analyzed (Wright et al., 2009; Wright and Son, 2007). We morphologically evaluated NMJ innervation by quantifying five different NMJ phenotypes at individual synapses. For each hemidiaphragm/animal, we quantified 200–300 NMJs across the entire hemidiaphragm, and we expressed the data for each NMJ phenotype as the percentage of total NMJs. We performed this analysis on 3–4 animals per group. Each individual animal is represented by a separate circle or triangle in Fig. 3M. We conducted this NMJ morphological analysis to confirm that there was no diaphragm denervation that could have resulted from factors such as PhMN damage or even PhMN death, as well as to show that LAR peptide administration did not impact diaphragm innervation by PhMNs.

3.7.9. Spinal cord and brainstem dissection—Rats were euthanized with Euthasol. After the diaphragms were excised, animals were perfused transcardially 8 weeks after injury with saline, followed by cold 4% paraformaldehyde. After post-fixation in the same fixative overnight, tissues were washed with 1xPBS and transferred to 30% sucrose solution in 1xPBS.

3.7.10. Immunohistochemistry—Spinal cord tissue extending from 10 mm rostral to the lesion to 10 mm caudal to the lesion (20 mm long, containing lesion area) was embedded in OCT and cryosectioned parasagittally on a Microm HM550 cryostat Microtome (Thermo Scientific) (40 μm thick). The free-floating sections were blocked/permeabilized with a solution of 5% Normal Goat Serum (Vector Laboratories, Burlingame, California), 0.2% Triton X-100 (Amresco, Solon, Ohio), diluted in PBS (primary and secondary antibodies were diluted in this solution as well) for 1 h at room temperature and then processed with primary antibodies at 4 °C overnight using procedures for immunocytochemistry, as described previously. Multiple primary antibodies were used in combination, including rabbit glial fibrillary acidic protein (GFAP) (1:500, RRID: AB_10013382, Dako), rabbit-anti-dsRed (1:500, Living Colors DsRed pAb, RRID: AB_10013483; Takara Bio USA, Mountain View, CA, USA) to enhance mCherry fluorescence, goat-anti-CTB (1:10,000; RRID: AB_10013220; List Biological Laboratories), mouse-anti-vesicular glutamate transporter 2 (1:250, RRID: AB_2187552; MilliporeSigma), rabbit-anti-5-hydroxy-tryptamine (5-HT; 1:15,000, RRID: AB_572263; ImmunoStar, Hudson, WI, USA). All secondary antibodies were used at 1:200 dilution for 1 h at room temperature and included: Alexa Fluor 647 AffiniPure Donkey anti-mouse, Alexa Fluor 488 AffiniPure donkey anti-goat, Alexa Fluor 647-conjugated donkey anti-goat, Alexa Fluor 488 AffiniPure donkey anti-rabbit (Jackson Immuno-Research Laboratories), and Alexa Fluor 594-conjugated donkey anti-rabbit (Abeam, Cambridge, MA, USA). The sections were mounted, dehydrated, covered with FluorSave™ Reagent (Millipore) and then added with cover slips. Stained sections were examined using a Leica SP8 confocal microscope (Leica Microsystems Inc., Buffalo Grove, IL). Image analysis was performed using Image J (NIH), as described previously (Urban et al., 2019a).

3.7.11. Counts of transduced rVRG neurons—To quantify numbers of AAV-mCherry transduced rVRG neuron cell bodies, 40 μm transverse sections of the medulla were imaged with a Zeiss Axio M2 Imager (Carl Zeiss Inc.). Images were then optically "stitched" by MetaMorph software (Molecular Devices; RRID: SCR_002368) to generate a complete image of the entire medulla section. The number of $mCherry^+$ transduced neurons in the rVRG per section were counted and averaged over multiple sections to obtain a single value for each animal.

3.7.12. Lesion size measurement—Lesion edge was defined as the interface between the GFAP-negative and GFAP-positive regions surrounding the lesion core. GFAP-negative tissue was defined as tissue that had little GFAP immunoreactivity, with few GFAP-positive cells or processes. GFAP-positive processes formed a defined boundary between GFAP-positive and GFAP-negative locations. Lesion borders were outlined manually based on images taken with a 20× objective lens. In each quantified sagittal section, rostral-caudal distance between the rostral and caudal lesion borders was measured at three locations (i.e. at dorsal, medial and rostral portions of the lesion in the sagittal section) using the NIH ImageJ analysis software, and three sections were averaged within an individual animal.

3.7.13. Spinal cord cresyl violet staining—40 μm transverse spinal cord sections were retrieved from the −20 °C freezer and dried at room temperature overnight. Slides were

then dipped in dH_2O for 30 s. Slides were next placed into a cresyl violet solution (0.4% cresyl violet, 6% 1 M sodium acetate, 34% 1 M acetic acid) for 18 min. Finally, slides were placed in baths of dH_2O, 70% ethanol, 95% ethanol, 100% ethanol and xylene. Slides were then mounted with poly-mount xylene (Polysciences, Warrington, Pennsylvania) and coverslips were added. Slides were then kept at room temperature for analysis.

3.7.14. Analysis of rVRG axon regeneration and sprouting—To visualize rVRG axons in animals with either ipsilateral or contralateral injections of AAV2-mCherry into the rVRG, sagittal sections were enhanced with a rabbit Living Colors DsRed Polyclonal antibody 1:500 (Takara Bio Company) and an Alexa-594-conjugated secondary antibody. For mCherry-labeled axon regeneration quantification (i.e. in rats injected with mCherry into ipsilateral rVRG), in the sagittal sections of cervical spinal cord containing the lesion site, the average number of mCherry-labeled axons that traversed through various distances were counted at the lesion site and in intact rostral and caudal spinal cord, using rostral lesion-intact border as the distance starting point (Urban et al., 2019b). For this rVRG axon regeneration quantification, we counted numbers of rVRG axon profiles that crossed a straight line (running from the dorsal to ventral part of the section) placed at each of the rostral-caudal distances presented in the graph in Fig. 5H. The same $mCherry^+$ axon could be counted at multiple distances (or even at the same distance because of branching and/or uturns). With this quantification, we are counting numbers of axon profiles at various rostral-caudal distances to assess density of rVRG axon growth.

For quantification of rVRG axon sprouting within the PhMN pool (i.e. in animals injected with AAV2-mCherry into contralateral rVRG), we quantified axon profile numbers within a constant-area size box (500 μm × 500 μm) at the location of CTB-labeled PhMNs on the side of C2 hemisection. Numbers of mCherry-labeled rVRG axons were obtained and averaged separately at C3, C4 and C5 regions of spinal cord: +1.5 (mm), +3.0 (mm), and + 4.5 (mm), respectively (Urban et al., 2019b). 4–5 sections were analyzed per rat, and 4–5 rats per group were quantified. Similar to rVRG axon regeneration analysis described above, the same rVRG axon could be counted more than once in this area box because of branching and/or because the axon exited and re-entered the 40 μm tissue section in the z-plane and/or x-y plane.

For both rVRG axon regeneration and rVRG axon sprouting, we present results as axon profiles. We identified an axon profile quantitatively as a continuous segment of mCherry-labeled axon that measures at least 10 μm in length.

3.7.15. Analysis of putative rVRG-PhMN monosynaptic connections—To quantify putative monosynaptic connections between presynaptic $mCherry^+$/Vesicular Glutamate Transporter 2 $(VGLUT2)^+$ rVRG axon terminals and post-synaptic CTB^+ PhMNs, longitudinal sections were triple immunostained with antibodies directed against Living Colors DsRed, VGLUT2 (Sigma) and Cholera Toxin B Subunit (List Biological Laboratories). For quantification of the number of putative monosynaptic connections at C3, C4 and C5 regions ipsilateral to the lesion, mCherry/VGLUT2 double-positive signals directly pre-synaptic to the somata of CTB^+ PhMNs were identified under orthogonal view in single-z confocal images (Urban et al., 2019b). We confirmed overlay of the VGLUT2

and mCherry signals in both the x-y and z planes. Using the same approach, we also quantified numbers of putative mCherry^{-}/VGlut2^{+} excitatory synapses onto CTB^{+} PhMNs (from non-rVRG excitatory neurons) at C3 on the side of hemisection.

3.7.16. Analysis of serotonergic axons—For serotonin axon labeling, parasagittal sections were immunostained with a rabbit anti-5-HT antibody (ImmunoStar) and Alexa-488-conjugated secondary antibody. For serotonergic axon quantification, the individual fibers stained by 5-HT antibody within a constant-area size box (500 μm × 500 μm) at the location of CTB-labeled PhMNs at C3, C4 and C5 regions were traced and the total length of all traced 5-HT axons was calculated from two random sections in each rat. Specifically, this sprouting quantification was performed within the ipsilateral PhMN pool on the side of C2 hemisection (Urban et al., 2019a).

3.7.17. Statistical analysis—All data are presented as the mean ± SEM. OriginPro 8.0 (OriginLab Corp.) was used for all statistical analysis. Data were analyzed with a one-way analysis of variance followed by a Tukey's multiple comparison test or a two-tailed Student's *t*-test. Pearson Correlation was used to examine correlation. P value <0.05 was considered significant.

Acknowledgments

We would like to thank Drs. Michael Lane and Tatiana Bezdudnaya for valuable discussions.

Funding

This work was supported by the National Institute of Neurological Disorders and Stroke (R01NS079702 to A.C.L.; R01NS105961, R01NS079432, R01EY024575 to S.L.), the Craig H. Neilsen Foundation (grant 476686 to A.C.L.), and the Shriners Hospital for Pediatric Research Foundation (grants SHC-85100, 85112-PHI-18 to S.L.; grants SHC 84051, SHC 86000 to G.M.S.).

Abbreviations:

AAV2	Adeno-associated virus serotype 2
C2 (3, 4, 5, etc.)	Cervical spinal cord level 2 (3, 4, 5, etc.)
CMAP	Compound muscle action potential
CNS	Central nervous system
CSPG	Chondroitin sulfate proteoglycan
CTB	Cholera toxin subunit B
ECM	Extracellular matrix
EMG	Electromyography
GAG	Glyeosaminoglyean
GFAP	Glial fibrillary acidic protein
LAR	Leukocyte common antigen-related

NMJ	Neuromuscular junction
PhMN	Phrenic motor neuron
RPTP	Receptor protein tyrosine phosphatase
rVRG	Rostral ventral respiratory group
SCI	Spinal cord injury
VGLUT2	Vesicular glutamate transporter 2
5-HT	5-hydroxytiyptamine

References

Ahuja CS, et al., 2017 Traumatic spinal cord injury. Nat. Rev. Dis. Primers 3, 17018. [PubMed: 28447605]

Alilain WJ, et al., 2011 Functional regeneration of respiratory pathways after spinal cord injury. Nature 475, 196–200. [PubMed: 21753849]

Anderson MA, et al., 2016 Astrocyte scar formation aids central nervous system axon regeneration. Nature 532, 195–200. [PubMed: 27027288]

Bareyre FM, et al., 2004 The injured spinal cord spontaneously forms a new intraspinal circuit in adult rats. Nat. Neurosci 7, 269–277. [PubMed: 14966523]

Barros CS, et al., 2011 Extracellular matrix: functions in the nervous system. Cold Spring Harb. Perspect. Biol 3, a005108. [PubMed: 21123393]

Bartus K, et al., 2012 Chondroitin sulphate proteoglycans: key modulators of spinal cord and brain plasticity. Exp. Neurol 235, 5–17. [PubMed: 21871887]

Beller JA, Snow DM, 2014 Proteoglycans: road signs for neurite outgrowth. Neural Regen. Res 9, 343–355. [PubMed: 25206822]

Benarroeh EE, 2015 Extracellular matrix in the CNS: dynamic structure and dinical correlations. Neurology. 85, 1417–1427. [PubMed: 26400579]

Bezdudnaya T, et al., 2017 Supraspinal respiratory plasticity following acute cervical spinal cord injury. Exp. Neurol 293, 181–189. [PubMed: 28433644]

Boulenguez P, et al., 2007 Specific and artifactual labeling in the rat spinal cord and medulla after injection of monosynaptic retrograde tracers into the diaphragm. Neurosci. Lett 417, 206–211. [PubMed: 17412505]

Bradbury EJ, et al., 2002 Chondroitinase ABC promotes functional recovery after spinal cord injury. Nature 416, 636–640. [PubMed: 11948352]

Burda JE, Sofroniew MV, 2014 Reactive gliosis and the multicellular response to CNS damage and disease. Neuron 81, 229–248. [PubMed: 24462092]

Charsar BA, et al., 2019 AAV2-BDNF promotes respiratory axon plasticity and recovery of diaphragm function following spinal cord injury. FASEB J. 33, 13775–13793. [PubMed: 31577916]

Cregg JM, et al., 2014 Functional regeneration beyond the glial scar. Exp. Neurol 253, 197–207. [PubMed: 24424280]

Dale-Nagle EA, et al., 2010 Spinal plasticity following intermittent hypoxia: implications for spinal injury. Ann. N. Y. Acad. Sci 1198, 252–259. [PubMed: 20536940]

Davies JE, et al., 2006 Astrocytes derived from glial-restricted precursors promote spinal cord repair. J. Biol 5, 7. [PubMed: 16643674]

Davies JE, et al., 2008 Transplanted astrocytes derived from BMP- or CNTF-treated glial-restricted precursors have opposite effects on recovery and allodynia after spinal cord injury. J. Biol 7, 24. [PubMed: 18803859]

Dickendesher TL, et al., 2012 NgR1 and NgR3 are receptors for chondroitin sulfate proteoglycans. Nat. Neurosci 15, 703–712. [PubMed: 22406547]

Dyck S, et al., 2018 Perturbing chondroitin sulfate proteoglycan signaling through LAR and PTPsigma receptors promotes a beneficial inflammatory response following spinal cord injury. J. Neuroinflammation 15, 90. [PubMed: 29558941]

Dyck S, et al., 2019 LAR and PTPsigma receptors are negative regulators of oligodendrogenesis and oligodendrocyte integrity in spinal cord injury. Glia. 67, 125–145. [PubMed: 30394599]

Falnikar A, et al., 2015 Therapeutically targeting astrocytes with stem and progenitor cell transplantation following traumatic spinal cord injury. Brain Res. 1619, 91–103. [PubMed: 25251595]

Fawcett JW, 2015 The extracellular matrix in plasticity and regeneration after CNS injury and neurodegenerative disease. Prog. Brain Res 218, 213–226. [PubMed: 25890139]

Fisher D, et al., 2011 Leukocyte common antigen-related phosphatase is a functional receptor for chondroitin sulfate proteoglycan axon growth inhibitors. J. Neurosci 31, 14051–14066. [PubMed: 21976490]

Franco SJ, Muller U, 2011 Extracellular matrix functions during neuronal migration and lamination in the mammalian central nervous system. Dev. Neurobiol 71, 889–900. [PubMed: 21739613]

Fry EJ, et al., 2010 Corticospinal tract regeneration after spinal cord injury in receptor protein tyrosine phosphatase sigma deficient mice. Glia. 58, 423–433. [PubMed: 19780196]

Fuller DD, Mitchell GS, 2017 Respiratory neuroplasticity - overview, significance and future directions. Exp. Neurol 287, 144–152. [PubMed: 27208699]

Garcia-Alias G, et al., 2009 Chondroitinase ABC treatment opens a window of opportunity for task-specific rehabilitation. Nat. Neurosci 12, 1145–1151. [PubMed: 19668200]

Ghosh B, et al., 2018 Local BDNF delivery to the injured cervical spinal cord using an engineered hydrogel enhances diaphragmatic respiratory function. J. Neurosci 38, 5982–5995. [PubMed: 29891731]

Goshgarian HG, 2003. The crossed phrenic phenomenon: a model for plasticity in the respiratory pathways following spinal cord injury. J. Appl. Physiol 94, 795–810 (1985).

Haas C, Fischer I, 2013 Human astrocytes derived from glial restricted progenitors support regeneration of the injured spinal cord. J. Neurotrauma 30, 1035–1052. [PubMed: 23635322]

Haas C, et al., 2012 Phenotypic analysis of astrocytes derived from glial restricted precursors and their impact on axon regeneration. Exp. Neurol 233, 717–732. [PubMed: 22101004]

Hamby ME, Sofroniew MV, 2010 Reactive astrocytes as therapeutic targets for CNS disorders. Neurotherapeutics 7, 494–506. [PubMed: 20880511]

Han KA, et al., 2016 Emergent synapse organizers: LAR-RPTPs and their companions. Int. Rev. Cell Mol. Biol 324, 39–65. [PubMed: 27017006]

Hill CE, et al., 2004 Acute transplantation of glial-restricted precursor cells into spinal cord contusion injuries: survival, differentiation, and effects on lesion environment and axonal regeneration. Exp. Neurol 190, 289–310. [PubMed: 15530870]

James ND, et al., 2015 Chondroitinase gene therapy improves upper limb function following cervical contusion injury. Exp. Neurol 271, 131–135. [PubMed: 26044197]

Kamada T, et al., 2011 Transplantation of human bone marrow stromal cell-derived Schwann cells reduces cystic cavity and promotes functional recovery after contusion injury of adult rat spinal cord. Neuropathology 31, 48–58. [PubMed: 20573032]

Keough MB, et al., 2016 An inhibitor of chondroitin sulfate proteoglycan synthesis promotes central nervous system remyelination. Nat. Commun 7, 11312. [PubMed: 27115988]

Kondo S, et al., 2010 Regulatory role of leukocyte-common-antigen-related molecule (LAR) in thymocyte differentiation. Eur. J. Immunol 40, 1296–1302. [PubMed: 20186877]

Kwok JC, et al., 2011 Extracellular matrix and perineuronal nets in CNS repair. Dev Neurobiol 71, 1073–1089. [PubMed: 21898855]

Lane MA, et al., 2008a Respiratory neuroplasticity and cervical spinal cord injury: translational perspectives. Trends Neurosci. 31, 538–547. [PubMed: 18775573]

Lane MA, et al., 2008b Cervical prephrenic interneurons in the normal and lesioned spinal cord of the adult rat. J. Comp. Neurol 511, 692–709. [PubMed: 18924146]

Lane MA, et al., 2009 Spinal circuitry and respiratory recovery following spinal cord injury. Respir. Physiol. Neurobiol 169, 123–132. [PubMed: 19698805]

Lang BT, et al., 2015 Modulation of the proteoglycan receptor PTPsigma promotes recovery after spinal cord injury. Nature 518, 404–408. [PubMed: 25470046]

Laskowski MB, Sanes JR, 1987 Topographic mapping of motor pools onto skeletal muscles. J. Neurosci. 7, 252–260. [PubMed: 3543250]

Li K, et al., 2014 Overexpression of the astrocyte glutamate transporter GLT1 exacerbates phrenic motor neuron degeneration, diaphragm compromise, and forelimb motor dysfunction following cervical contusion spinal cord injury. J. Neurosci 34, 7622–7638. [PubMed: 24872566]

Li K, et al., 2015a Transplantation of glial progenitors that overexpress glutamate transporter GLT1 preserves diaphragm function following cervical SCI. Mol. Ther 23, 533–548. [PubMed: 25492561]

Li K, et al., 2015b Human iPS cell-derived astrocyte transplants preserve respiratory function after spinal cord injury. Exp. Neurol 271, 479–492. [PubMed: 26216662]

Li S, Strittmatter SM, 2003 Delayed systemic Nogo-66 receptor antagonist promotes recovery from spinal cord injury. J. Neurosci 23, 4219–4227. [PubMed: 12764110]

Mantilla CB, et al., 2017 Impact of glutamatergic and serotonergic neurotransmission on diaphragm muscle activity after cervical spinal hemisection. J. Neurophysiol 118, 1732–1738. [PubMed: 28659464]

Meves JM, Zheng B, 2014 Extrinsic inhibitors in axon sprouting and functional recovery after spinal cord injury. Neural Regen. Res 9, 460–461. [PubMed: 25206838]

Nicaise C, et al., 2012a Phrenic motor neuron degeneration compromises phrenic axonal circuitry and diaphragm activity in a unilateral cervical contusion model of spinal cord injury. Exp. Neurol 235, 539–552. [PubMed: 22465264]

Nicaise C, et al., 2012b Degeneration of phrenic motor neurons induces long-term diaphragm deficits following mid-cervical spinal contusion in mice. J. Neurotrauma 29, 2748–2760. [PubMed: 23176637]

Nicaise C, et al., 2013 Early phrenic motor neuron loss and transient respiratory abnormalities after unilateral cervical spinal cord contusion. J. Neurotrauma 30, 1092–1099. [PubMed: 23534670]

Ohtake Y, et al., 2016 Two PTP receptors mediate CSPG inhibition by convergent and divergent signaling pathways in neurons. Sci. Rep 6, 37152. [PubMed: 27849007]

Ohtake Y, et al., 2017 Protein tyrosine phosphatase sigma regulates autoimmune encephalomyelitis development. Brain Behav. Immun 65, 111–124. [PubMed: 28559011]

Ohtake Y, et al., 2018 Diverse functions of protein tyrosine phosphatase sigma in the nervous and immune systems. Exp. Neurol 302, 196–204. [PubMed: 29374568]

Park KK, et al., 2010 PTEN/mTOR and axon regeneration. Exp. Neurol 223, 45–50. [PubMed: 20079353]

Perrin FE, Noristani HN, 2019 Serotonergic mechanisms in spinal cord injury. Exp. Neurol 318, 174–191. [PubMed: 31085200]

Pike KA, Tremblay ML, 2013 Regulating naive and memory CDS T cell homeostasis-a role for protein tyrosine phosphatases. FEBS J. 280, 432–444. [PubMed: 22458809]

Ramer LM, et al., 2014 Restoring function after spinal cord injury: towards clinical translation of experimental strategies. Lancet Neurol. 13, 1241–1256. [PubMed: 25453463]

Robinson J, Lu P, 2017 Optimization of trophic support for neural stem cell grafts in sites of spinal cord injury. Exp. Neurol 291, 87–97. [PubMed: 28189728]

Roth BL, 2016 DREADDs for neuroscientists. Neuron 89, 683–694. [PubMed: 26889809]

Sharma K, et al., 2012 Scar-mediated inhibition and CSPG receptors in the CNS. Exp. Neurol 237, 370–378. [PubMed: 22836147]

Shen Y, et al., 2009 PTPsigma is a receptor for chondroitin sulfate proteoglycan, an inhibitor of neural regeneration. Science 326, 592–596. [PubMed: 19833921]

Shih CH, et al., 2014 Astroglial-derived periostin promotes axonal regeneration after spinal cord injury. J. Neurosci 34, 2438–2443. [PubMed: 24523534]

Silver J, et al., 2014 Central nervous system regenerative failure: role of oligodendrocytes, astrocytes, and microglia. Cold Spring Harb. Perspect. Biol 7, a020602. [PubMed: 25475091]

Smith GM, Silver J, 1988 Transplantation of immature and mature astrocytes and their effect on scar formation in the lesioned central nervous system. Prog. Brain Res 78, 353–361. [PubMed: 3247435]

Smith GM, et al., 1986 Changing role of forebrain astrocytes during development, regenerative failure, and induced regeneration upon transplantation. J. Comp. Neurol 251, 23–43. [PubMed: 3760257]

Smith GM, et al., 1987 Astrocyte transplantation induces callosal regeneration in postnatal acallosal mice. Ann. N. Y. Acad. Sci 495, 185–206. [PubMed: 3474941]

Smith GM, et al., 1990 Maturation of astrocytes in vitro alters the extent and molecular basis of neurite outgrowth. Dev. Biol 138, 377–390. [PubMed: 2318341]

Sofroniew MV, 2015 Astrocyte barriers to neurotoxic inflammation. Nat. Rev. Neurosci 16, 249–263. [PubMed: 25891508]

Sofroniew MV, 2018 Dissecting spinal cord regeneration. Nature 557, 343–350. [PubMed: 29769671]

Sperry RW, 1963 Chemoaffmity in the orderly growth of nerve Fiber patterns and connections. Proc. Natl. Acad. Sci. U. S. A 50, 703–710. [PubMed: 14077501]

Streeter KA, et al., 2020 Mid-cervical interneuron networks following high cervical spinal cord injury. Respir. Physiol. Neurobiol 271, 103305. [PubMed: 31553921]

Takahashi H, Craig AM, 2013 Protein tyrosine phosphatases PTPdelta, PTPsigma, and LAR: presynaptic hubs for synapse organization. Trends Neurosci. 36, 522–534. [PubMed: 23835198]

Terszowski G, et al., 2001 Within the hemopoietic system, LAR phosphatase is a T cell lineage-specific adhesion receptor-like protein whose phosphatase activity appears dispensable for T cell development, repertoire selection and function. Eur. J. Immunol 31, 832–840. [PubMed: 11241288]

Tonks NK, 2006 Protein tyrosine phosphatases: from genes, to function, to disease. Nat. Rev. Mol. Cell Biol 7, 833–846. [PubMed: 17057753]

Tran AP, et al., 2018 The biology of regeneration failure and success after spinal cord injury. Physiol. Rev 98, 881–917. [PubMed: 29513146]

Um JW, Ko J, 2013 LAR-RPTPs: synaptic adhesion molecules that shape synapse development. Trends Cell Biol. 23, 465–475. [PubMed: 23916315]

Urban MW, et al., 2018 Cell-type specific expression of constitutively-active Rheb promotes regeneration of bulbospinal respiratory axons following cervical SCI. Exp. Neurol 303, 108–119. [PubMed: 29453976]

Urban MW, et al., 2019a Protein tyrosine phosphatase sigma inhibitory peptide promotes recovery of diaphragm function and sprouting of Bulbospinal respiratory axons after cervical spinal cord injury. J. Neurotrauma 37, 572–579. [PubMed: 31392919]

Urban MW, et al., 2019b Long-distance axon regeneration promotes recovery of diaphragmatic respiratory function after spinal cord injury. eNeuro 6.

Urban MW, et al., 2020 Protein tyrosine phosphatase sigma inhibitory peptide promotes recovery of diaphragm function and sprouting of Bulbospinal respiratory axons after cervical spinal cord injury. J. Neurotrauma 37, 572–579. [PubMed: 31392919]

Warren PM, et al., 2014 Drawing breath without the command of effectors: the control of respiration following spinal cord injury. Respir. Physiol. Neurobiol 203, 98–108. [PubMed: 25149585]

Warren PM, et al., 2018 Rapid and robust restoration of breathing long after spinal cord injury. Nat. Commun. 9, 4843. [PubMed: 30482901]

Wong EC, et al., 1993 Leukocyte common antigen-related phosphatase (LRP) gene structure: conservation of the genomic organization of transmembrane protein tyrosine phosphatases. Genomics 17, 33–38. [PubMed: 8406469]

Wright MC, Son YJ, 2007 Ciliary neurotrophic factor is not required for terminal sprouting and compensatory reinnervation of neuromuscular synapses: re-evaluation of CNTF null mice. Exp. Neurol 205, 437–448. [PubMed: 17445802]

Wright MC, et al., 2009 Distinct muscarinic acetylcholine receptor subtypes contribute to stability and growth, but not compensatory plasticity, of neuromuscular synapses. J. Neurosci 29, 14942–14955. [PubMed: 19940190]

Wu CL, et al., 2017 Identification of function-regulating antibodies targeting the receptor protein tyrosine phosphatase sigma ectodomain. PLoS One 12, e0178489. [PubMed: 28558026]

Xie X, et al., 2020 Structural basis of liprin-alpha-promoted LAR-RPTP clustering for modulation of phosphatase activity. Nat. Commun 11, 169. [PubMed: 31924785]

Xu B, et al., 2015 Role of CSPG receptor LAR phosphatase in restricting axon regeneration after CNS injury. Neurobiol. Dis 73, 36–48. [PubMed: 25220840]

Yang T, et al., 1999 Leukocyte common anti gen-related tyrosine phosphatase receptor: increased expression and neuronal-type splicing in breast cancer cells and tissue. Mol. Carcinog 25, 139–149. [PubMed: 10365916]

Zheng Y, et al., 1998 Brainstem neurons projecting to the rostral ventral respiratory group (VRG) in the medulla oblongata of the rat revealed by co-application of NMDA and biocytin. Brain Res. 782, 113–125. [PubMed: 9519255]

Zholudeva LV, et al., 2017 Anatomical recruitment of spinal V2a interneurons into phrenic motor circuitry after high cervical spinal cord injury. J. Neurotrauma 34, 3058–3065. [PubMed: 28548606]

Zhu Y, et al., 2015 Hematogenous macrophage depletion reduces the fibrotic scar and increases axonal growth after spinal cord injury. Neurobiol. Dis 74, 114–125. [PubMed: 25461258]

Zimmer MB, et al., 2007 Effect of spinal cord injury on the respiratory system: basic research and current clinical treatment options. J. Spinal Cord. Med 30, 319–330. [PubMed: 17853653]

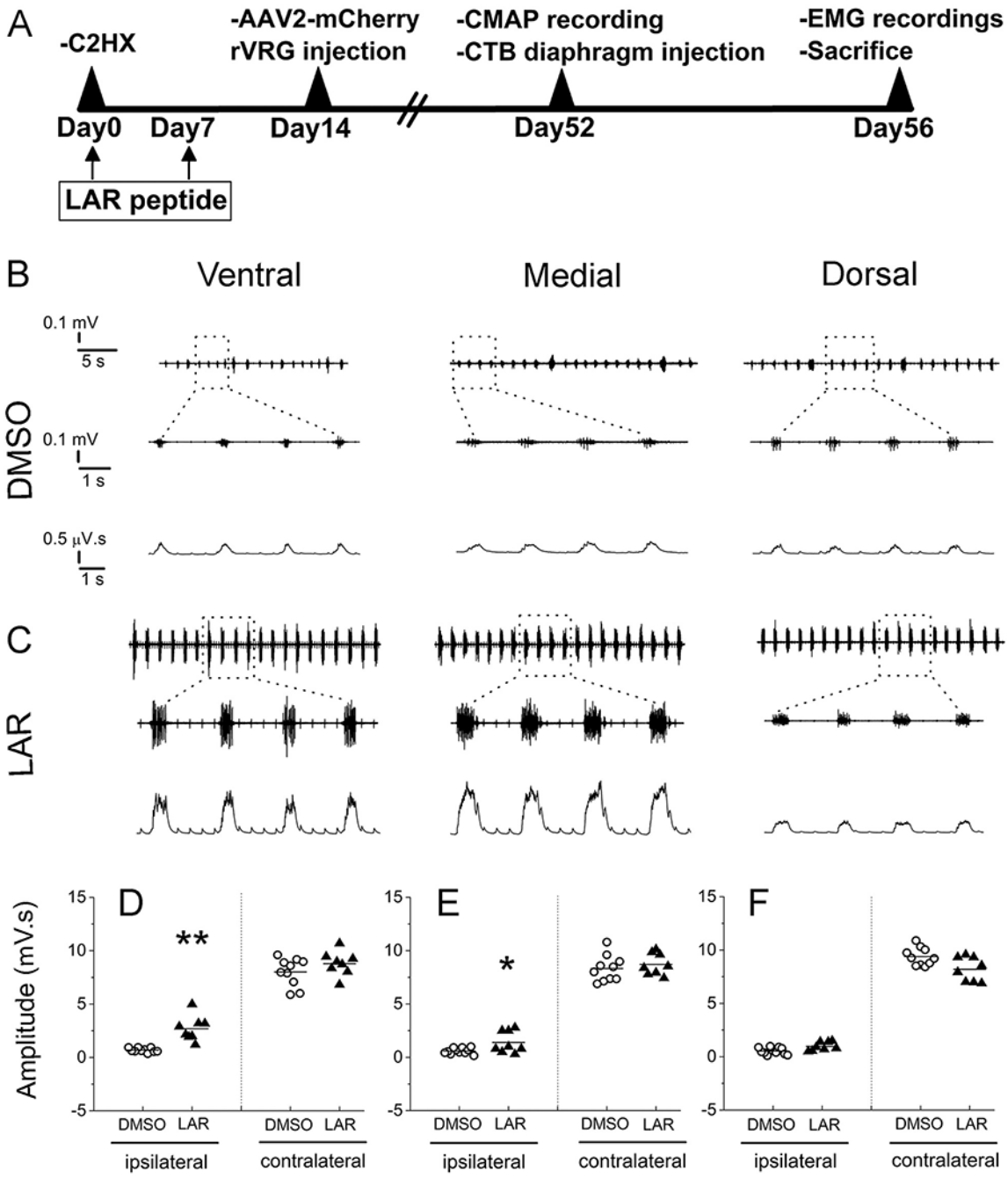

Fig. 1.

LAR peptide promoted recovery of diaphragm function after C2 hemisection SCI. (A) Timeline of experimental design. At 8 weeks post injury, EMG recordings were assessed at 3 sub-regions of both the ipsilateral and contralateral hemidiaphragm (dorsal, medial and ventral sub-regions) from C2 hemisection rats receiving either DMSO-only (B) or LAR peptide (C). (B, C) Representative EMG recordings from ipsilateral hemidiaphragm. Top: raw EMG traces; bottom: integrated signals. Quantification of integrated EMG amplitude 8

weeks after C2 hemisection at ventral (D) medial (E) and dorsal (F) sub-regions, $n = 8–10$ animals per group. Data represent mean ± SEM, $*P < 0.05$ vs the respective control.

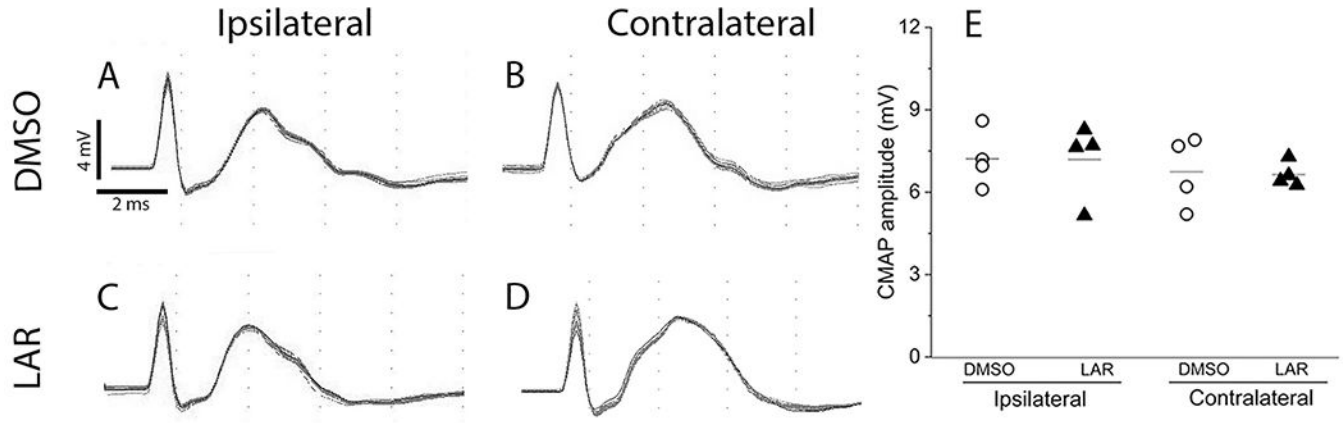

Fig. 2.

LAR peptide did not affect functional innervation of the diaphragm by PhMNs. Representative CMAP recordings obtained from the ipsilateral and contralateral hemidiaphragm of DMSO-only (A-B) and LAR peptide (C-D) groups. (E) Quantification of CMAP amplitudes showed no differences between the DMSO-only and LAR peptide groups or between ipsilateral and contralateral hemidiaphragm. $n = 4$ animals per group, $P > 0.05$.

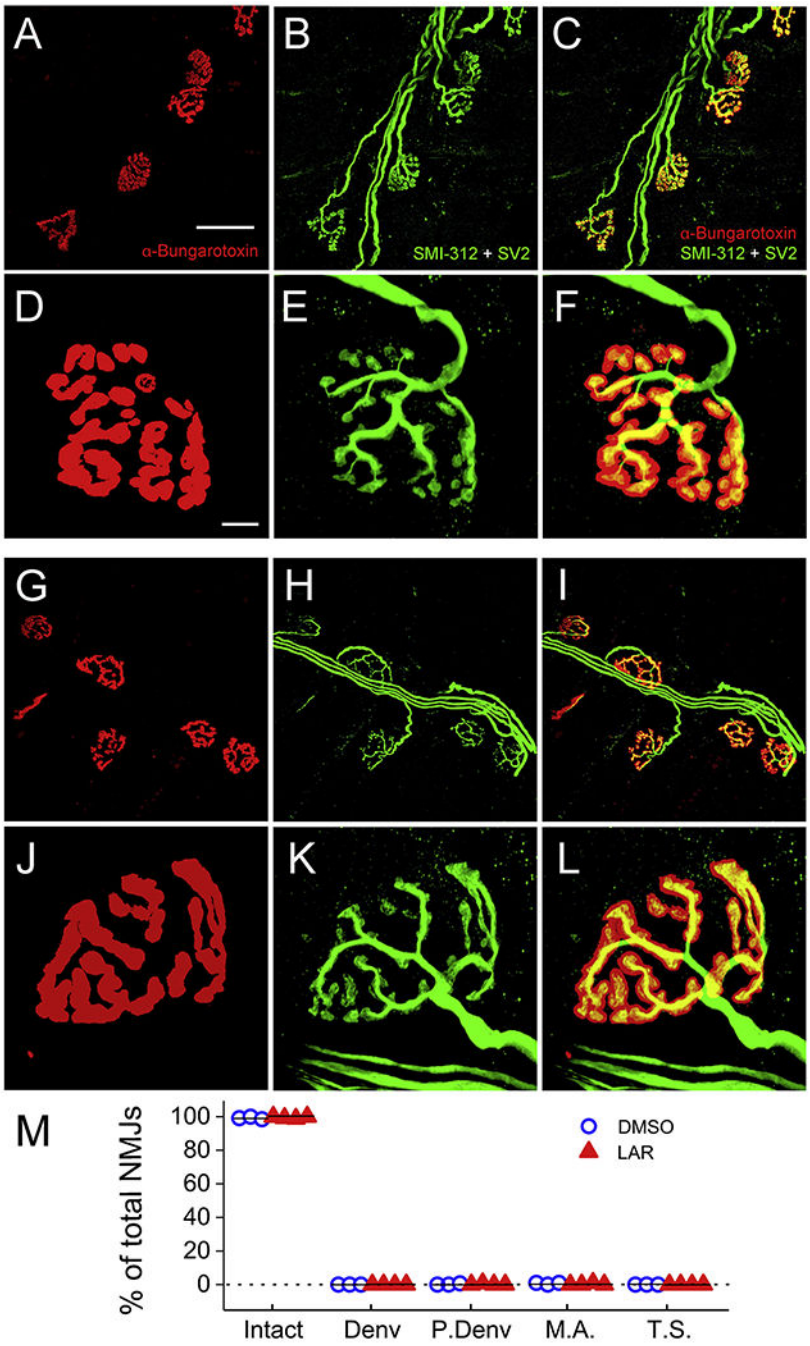

Fig. 3.

LAR peptide did not affect morphological innervation of the diaphragm by PhMNs. Whole-mount immunohistochemistry of diaphragm was used to label postsynaptic nicotinic acetylcholine receptors with AlexaFluor-conjugated alpha-bungarotoxin (red) and pre-synaptic phrenic motor axons all the way to their terminals with an antibody against neurofilament (SMI-312, green) and a second antibody against synaptic vesicle protein 2 (SV2, also green). As shown in representative confocal z-stacks, nearly all NMJs in ipsilateral hemidiaphragm were intact in C2 hemisection animals receiving either DMSO-

only (A-F) or LAR peptide (G-L). As shown in the higher magnification images, intact NMJs were characterized by complete apposition of the pre- and post-synaptic labeling. There were no differences in the percentages of intact, completely-denervated (Denv) or partially-denervated (P.Denv) NMJs, the portion of NMJs innervated by multiply phrenic motor axons (M.A.) or the percentage of NMJs with thin preterminal axons (T.S.) between rats treated with DMSO-only and LAR peptide (M), $n = 3$ for DMSO-only, $n = 4$ for LAR peptide. $P > 0.05$ vs the respective control. (For interpretation of the references to colour in this figure legend, the reader is referred to the web version of this article.)

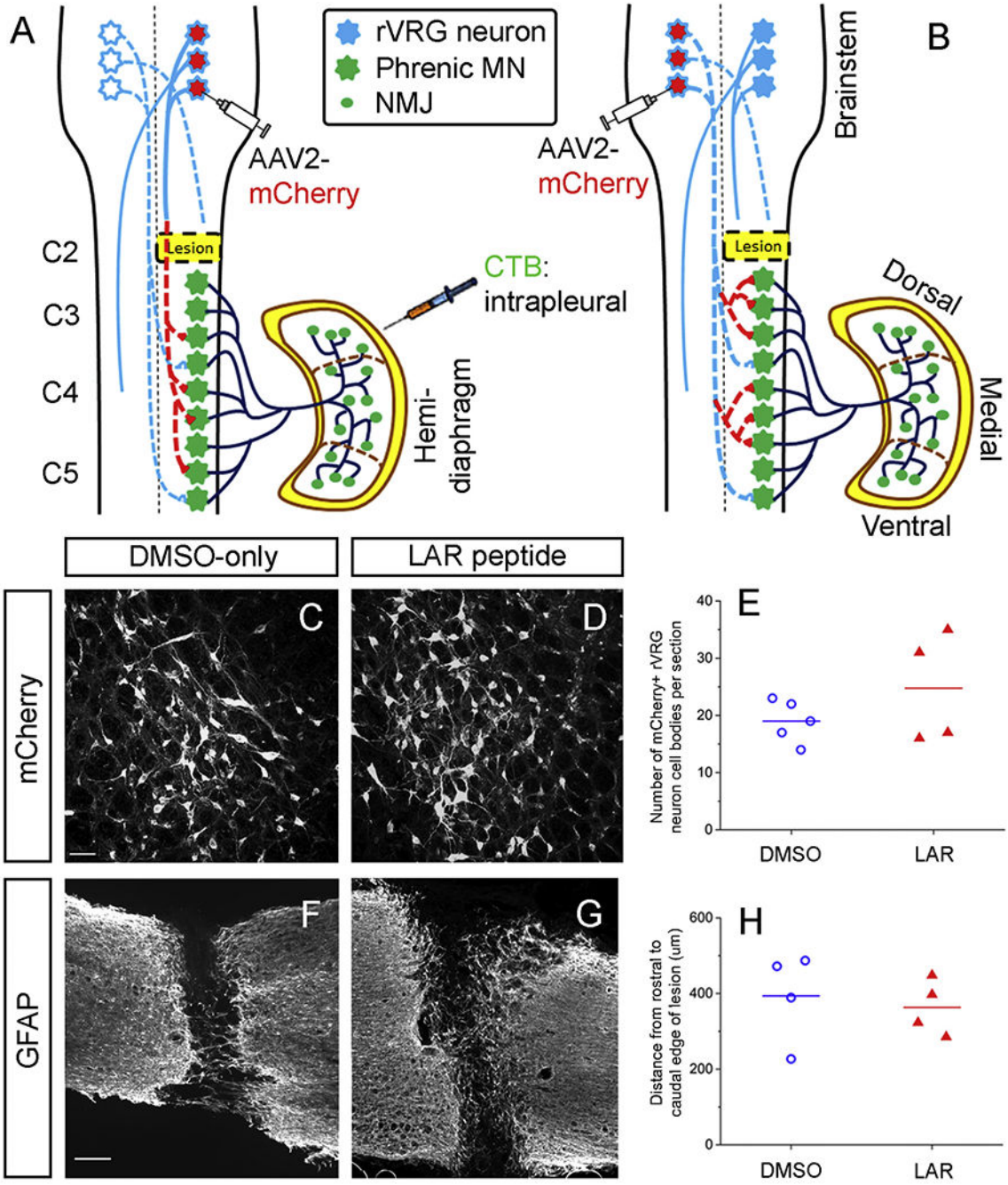

Fig. 4.

Labeling of rVRG-PhMN circuitiy. (A) To determine whether LAR peptide treatment promoted rVRG axon regeneration, we selectively transduced rVRG neurons within the medulla ipsilateral to the hemisection with AAV2-mCherry. (B) In a separate cohort of rats, we examined whether sprouting of spared rVRG axons originating in the contralateral medulla was induced by LAR peptide by injecting the AAV2-mCherry anterograde tracer into the contralateral rVRG and then quantifying sprouting of these axons within the PhMN pool on the side of the hemisection (i.e. contralateral to the location of their cell bodies). In

both cohorts, we intrapleurally injected Cholera Toxin B Subunit (CTB) to selectively label PhMN cell bodies within the cervical spinal cord. There was no difference in the number of AAV2-mCherry transduced rVRG neuron cell bodies in the medulla between the DMSO-only (C) and LAR peptide (D) groups ($P = 0.32$, $n = 4$ per group); quantification in (E). Sagittal spinal cord sections immunolabeled for GFAP from DMSO-only control (F) and LAR peptide (G) show that LAR peptide did not alter lesion size after C2 hemisection. (H) Quantification of GFAP-labeled sections shows no difference in lesion size as measured by the rostral-caudal distance from the rostral to caudal borders of the lesion ($P = 0.67$, $n = 4$ rats per group).

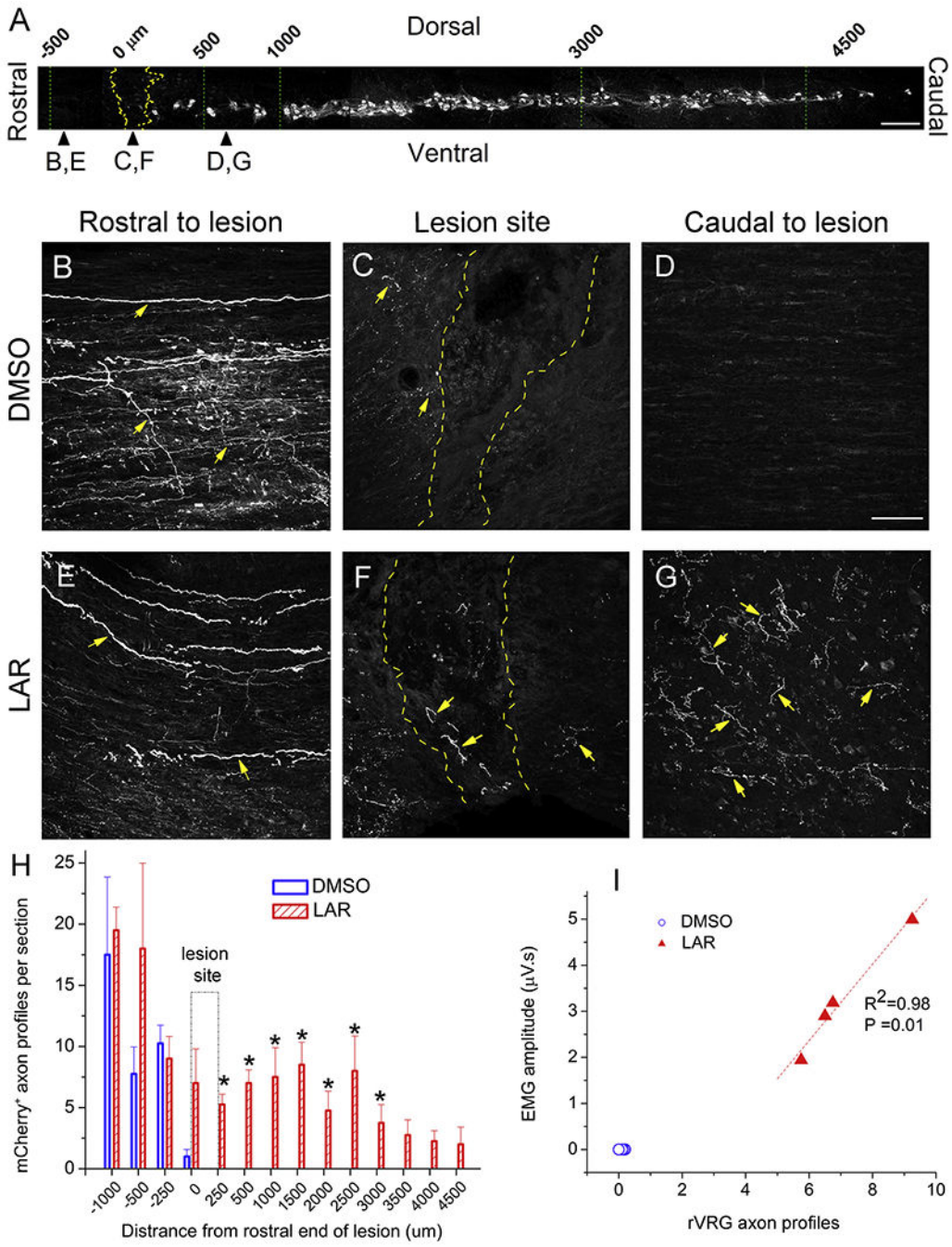

Fig. 5.

LAR peptide promoted rVRG axon regeneration through the lesion and into the intact caudal spinal cord. (A) Sagittal section of cervical spinal cord showing the columnar organization of CTB-labeled PhMNs extending from C3 to C5, the locations (i.e. rostral-caudal distances relative to the hemisection site) of rVRG axon growth analysis, and the location of the representative images in panels B-G; scale bar in (A): 250 μm. Representative images of sagittal sections from DMSO-only or LAR peptide treated rats injected with AAV2-mCherry into the ipsilateral rVRG: (B,E) rostral to lesion site, (C,F) lesion site, (D,G) caudal to lesion

site. These images from the two groups were always taken from the same rostral-caudal position/distance relative to the lesion epicenter. Yellow arrows in panels B-G denote mCheriy-labeled rVRG axons. Dotted yellow lines in panels C and F denote the rostral and caudal lesion-intact borders. Scale bar: 100 μm. (H) Quantification shows the numbers of ipsilateral-originating mCheriy-labeled rVRG axons at different locations in DMSO-only and LAR peptide group using the rostral end of the lesion as the rostral-caudal starting point. The indicated differences were compared between DMSO-only and LAR peptide groups at each distance ($n = 4$ animals per group, $*P < 0.05$). (I) Pearson Correlation was used to examine the correlation between the degree of rVRG axon regeneration at the C3 level and EMG amplitude in the corresponding ventral diaphragm subregion (correlation coefficient for linear fit, $R^2 = 0.98$, $P = 0.01$, $n = 4$ animals per group). (For interpretation of the references to colour in this figure legend, the reader is referred to the web version of this article.)

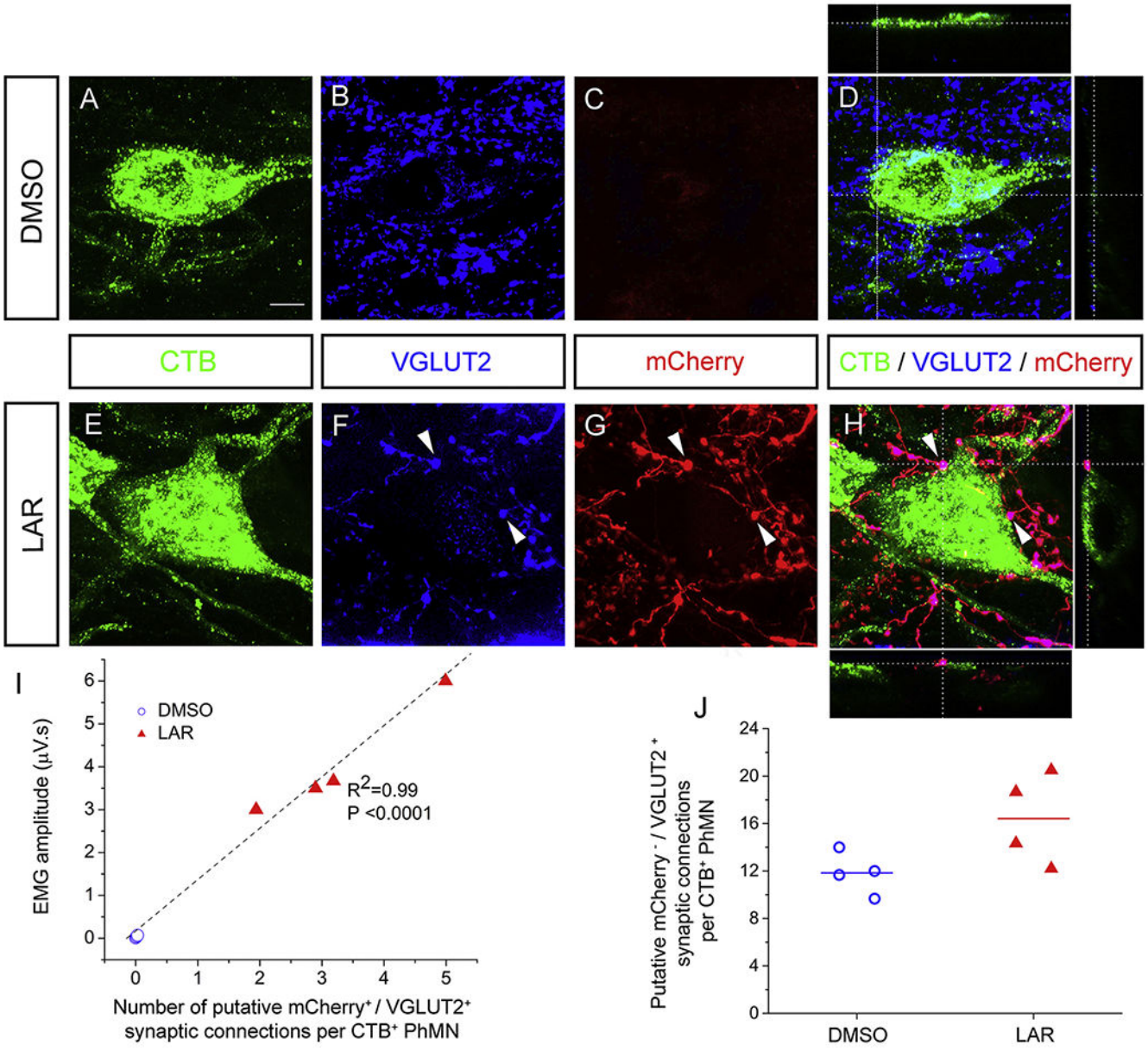

Fig. 6.

LAR peptide promoted putative monosynaptic connection between regenerating rVRG axon and PhMNs. We assessed the number of putative synaptic connections specifically between mCheriy/DsRed-positive rVRG axons and CTB-labeled PhMN cell bodies at level C3 with confocal acquisition of z-stacks and quantification of rVRG axon-PhMN contacts using single-Z section analysis to establish direct apposition of pre-synaptic VGLUT2+/mCheriy+ axon terminals and post-synaptic CTB^+ PhMNs. Representative images in panels A-H are compressed z-stacks. (A-D) We observed no putative rVRG-PhMN synapses in the DMSO-only control. (*E*-H) On the contrary, we observed large numbers of putative rVRG-PhMN synapses in the LAR peptide group. (I) Orthogonal projection shows $mCherry^+/VGLUT2^+$ excitatory rVRG axon terminals located directly presynaptic to the soma of a CTB^+ PhMN

(example putative connections denoted by arrowheads). Scale bar: 100 μm. Quantification of the number of these synaptic connections per individual PhMN at C3 plotted against the EMG amplitude from the corresponding ventral subregion in LAR peptide group (R^2 = 0.99; P < 0.0001, n = 4). (J) Quantification of the effects of LAR peptide on putative excitatory synapses from mCherry$^-$/VGLUT2$^+$ non-rVRG inputs per ipsilateral PhMN at C3 (P = 0.07, n = 4 rats per group).

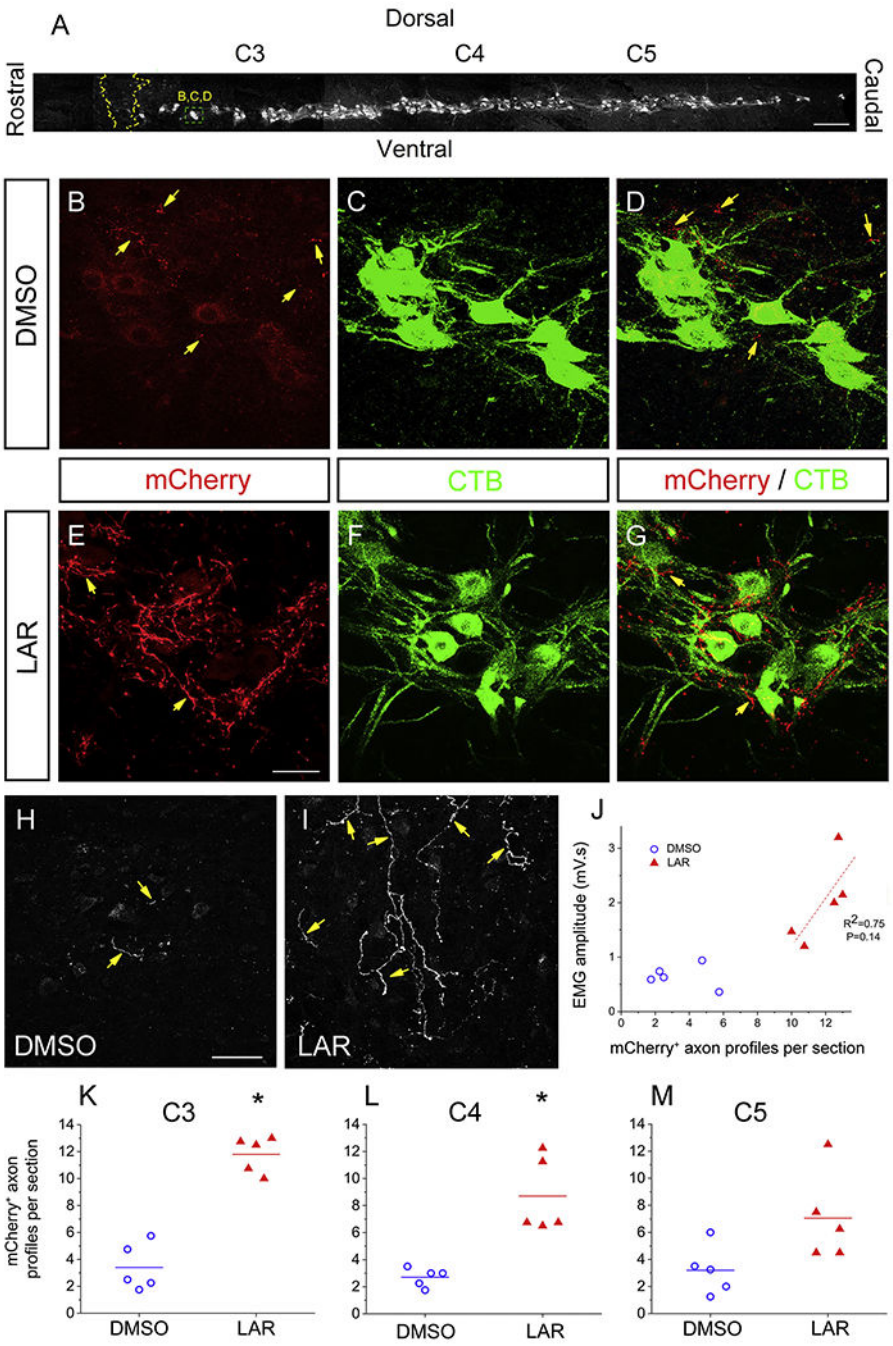

Fig. 7.

LAR peptide promoted sprouting of rVRG axons within the PhMN pool. (A) Sagittal section of cervical spinal cord showing the columnar organization of CTB-labeled PhMNs extending from C3 to C5, the locations of rVRG axon growth analysis, and the location of the representative images in panels B-D as well as E-G. Sagittal spinal cord sections were double-immunolabeled with DsRed (to enhance the mCherry signal) and CTB. We counted numbers of mCherry$^+$ fibers within the phrenic nucleus (i.e. the location of CTB$^+$ PhMNs) at distances of 1.5 mm, 3.0 mm and 4.5 mm caudal to the lesion that correspond to C3, C4

and C5 levels, respectively; scale bar in (A): 250 μm. Representative confocal images show PhMNs labeled with CTB that were surrounded by mCherry$^+$ rVRG axons. Contralateral-originating rVRG axons are present within the PhMN pool on the side of hemisection in both the DMSO-only (B-D) and LAR-peptide treated (E-G) conditions. (H, I) Yellow arrows indicate mCherry-labeled rVRG axons only. Scale bars: 100 μm. (F) The number of these mCherry$^+$ fibers in the LAR peptide group increased significantly compared to DMSO-only control at C3 (E-I, K) and C4 (L), but there was no significant difference at C5 (M) ($P < 0.05$). (G) Pearson Correlation was used to examine the correlation between the degree of rVRG axon sprouting at the C3 level and EMG amplitude in the corresponding ventral diaphragm subregion in the LAR peptide group (correlation coefficient for linear fit, $R^2 = 0.75$; $P = 0.14$, $n = 5$). (For interpretation of the references to colour in this figure legend, the reader is referred to the web version of this article.)

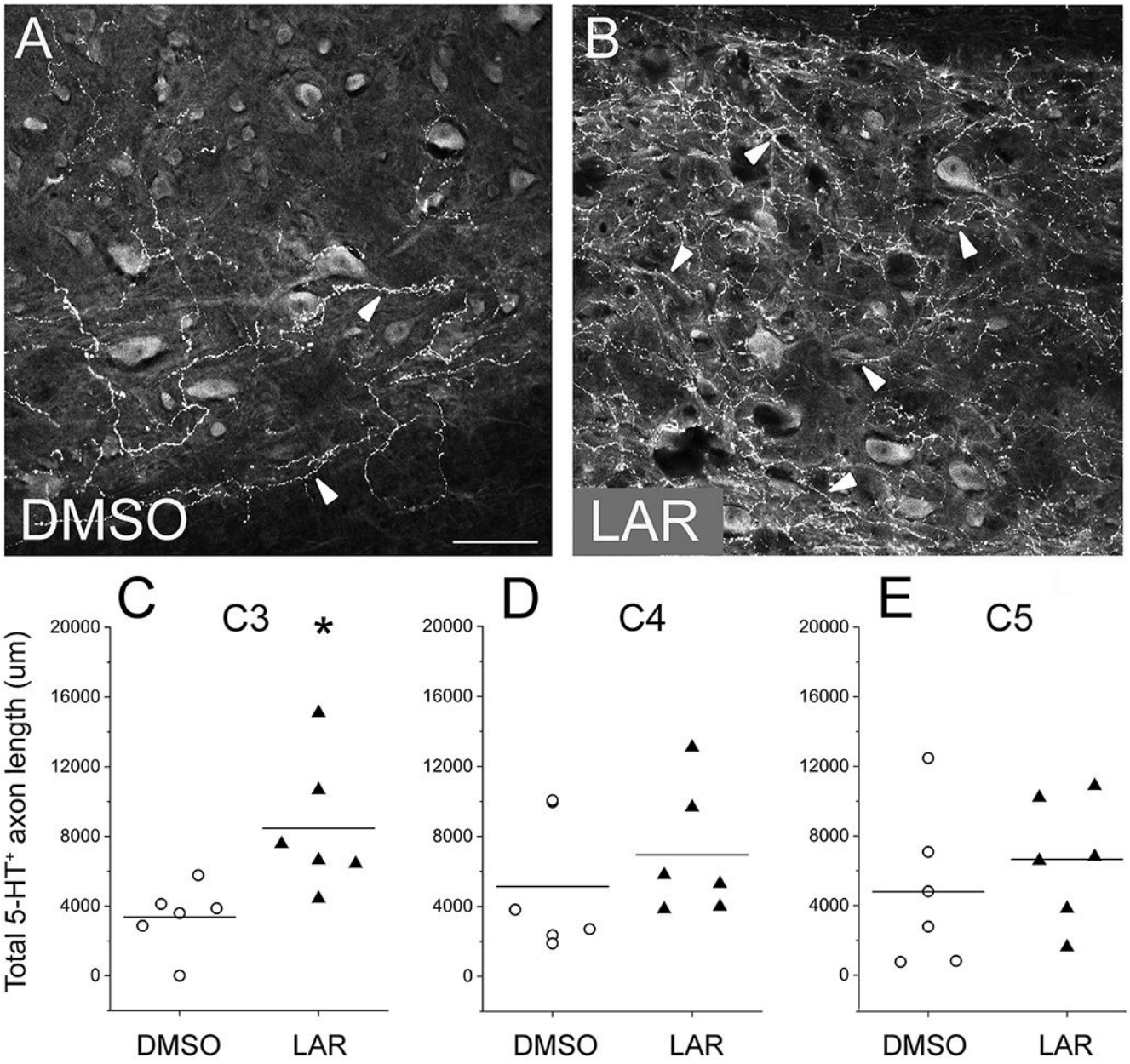

Fig. 8.

LAR peptide promoted sprouting of modulatoiy serotonergic axons within the PhMN pool. At 8 weeks after hemisection SCI, we assessed the density of serotonergic axon innervation of the PhMN pool on the side of injury by performing immunohistoehemistry for serotonin (5-HT) and quantifying the total length of 5-HT$^+$ axons. Sagittal sections of the cervical spinal cord show that, compared to DMSO-only control (A), LAR peptide significantly increased 5-HT axon sprouting within the ipsilateral phrenic nucleus at C3 (B—C) at 8 weeks post-injury ($n = 6$ animals per group, $*P = 0.02$). However, LAR peptide did not affect the density of 5-HT axon innervation of the ipsilateral PhMN pool at C4 (D; $P = 0.42$) or C5 (E; $P = 0.44$). Scale bar: 100 μm. Arrowheads indicate 5-HT$^+$ axons.